Chiral Nanoceramics

Jinchen Fan and Nicholas A. Kotov*

The study of different chiral inorganic nanomaterials has been experiencing rapid growth during the past decade, with its primary focus on metals and semiconductors. Ceramic materials can substantially expand the range of mechanical, optical, chemical, electrical, magnetic, and biological properties of chiral nanostructures, further stimulating theoretical, synthetic, and applied research in this area. An ever-expanding toolbox of nanoscale engineering and self-organization provides a chirality-based methodology for engineering of hierarchically organized ceramic materials. However, fundamental discoveries and technological translations of chiral nanoceramics have received substantially smaller attention than counterparts from metals and semiconductors. Findings in this research area are scattered over a variety of sources and subfields. Here, the diversity of chemistries, geometries, and properties found in chiral ceramic nanostructures are summarized. They represent a compelling materials platform for realization of chirality transfer through multiple scales that can result in new forms of ceramic materials. Multiscale chiral geometries and the structural versatility of nanoceramics are complemented by their high chiroptical activity, enantioselectivity, catalytic activity, and biocompatibility. Future development in this field is likely to encompass chiral synthesis, biomedical applications, and optical/electronic devices. The implementation of computationally designed chiral nanoceramics for biomimetic catalysts and quantum information devices may also be expected.

1. Background

Chirality is the geometric property that describes an object that is not non-superimposable upon its mirror image. A universal characteristic of an object's symmetry, it is observed at any length scale from subatomic particles to galaxies.[1] Since the discovery of molecular scale chirality of tartaric acid by Louis Pasteur in 1848,[2] it has become a constantly evolving branch of chemistry,[3] biology,[4] and physics[5] stimulating the development of an extensive toolbox for enantiopure materials.

Although chiral chemistry is most often associated with biomolecules,[6] enantiopure compounds are no longer a restricted to L-amino acids, D-sugars, and DNA and represents, perhaps, one of the most rapidly developing areas of nanotechnology. Chiroptical responses of most biomolecules are relatively weak and typically confined to the ultraviolet (UV) range (190–300 nm). Semiconductor and metallic nanostructures make possible an order-of-magnitude enhancement of chiroptical responses due to the high polarizability of these materials.[7] One of the first observations in this area was made by Schaaf and Whetten[8] who observed that individual gold clusters ≈0.5 nm in diameter stabilized with the tripeptide glutathione (glu–cys–gly) have circular dichroism (CD) in visible range. Moloney et al.[9] found similar effects for D- and L-penicillamine-capped CdS semiconductor nanoparticles (NPs), while Zhou et al.[10] confirmed these observation for D- and L-cysteine-stabilized CdTe NPs, as well as other semiconductor NPs.[11] About the same time, researchers also realized that 3D geometries of multiparticle constructs of NPs can also be asymmetric that affords both further enhancement of the chiroptical response and its tuning over a wide range of wavelengths.[12] These and other works opened the door to further studies of chiral inorganic nanomaterials resulting in a continuously emerging spectrum of chiral nanomaterials. The venue of applied research stimulated by these discoveries include biosensing,[13] chiral photonics,[14] optoelectronics,[15] biomolecule separation,[16] and, more recently, chiral catalysis.[17] Chiral nanostructures from ceramics, such as metal oxides, nitrides, carbides, silicates, etc., can certainly provide attractive alternatives to noble metals, and II–VI semiconductors dominating the current research for these applications. These new chiral materials may also stimulate other conceptual developments in this field related cellular responses,[18] drug delivery,[19] catalysis,[20] biomineralization,[21,98] magnetism,[22] astrophysics,[23] and geological processes.[24]

Ceramics are nonmetallic, inorganic solids that have been used by humans in the form of pottery as far back as 24 000 BC.[25] Ceramic materials commonly have high melting points, exceptional hardness and strength, considerable durability, low electrical and thermal conductivity, and

Prof. J. C. Fan, Prof. N. A. Kotov
Department of Chemical Engineering and
Department of Materials Science and Engineering
University of Michigan
Ann Arbor, MI 48109, USA
E-mail: Kotov@umich.edu
Prof. J. C. Fan
Shanghai Key Laboratory of Materials Protection and
Advanced Materials in Electric Power
College of Environmental and Chemical Engineering
Shanghai University of Electric Power
Shanghai 200090, China

The ORCID identification number(s) for the author(s) of this article can be found under https://doi.org/10.1002/adma.201906738.

ADVANCED
SCIENCE NEWS

www.advancedsciencenews.com

ADVANCED
MATERIALS

www.advmat.de

chemical inertness.[26,27] Traditional ceramics, composed of various combinations of clay and silica, refer to brick, pottery, glass, porcelain, tile, cement, and concrete that are present in everyday objects.[27] Advanced ceramics including alumina, zirconia, metal oxides, silicon nitride, boron nitride, silicon carbide, zeolite, etc. have played indispensable roles in modern manufacturing and engineering industry.[28]

In the early 19th century, French physicist Jean Baptiste Biot first discovered that single crystals of quartz could rotate plane-polarized light.[29] Quartz is a mineral with chiral crystal lattice which exists naturally as either dextrorotatory or levorotatory enantiomorphs.[30] Like quartz, a variety of other ceramics, such as zeolites also are known to have chiral crystal lattices that have been explored for their enantioselective adsorption,[31,152] asymmetric catalysis,[32] and chiroptical properties.[33] Besides utilization in optical devices, there is a growing understanding that surface interactions between amino acids and ceramic minerals is related to the origin of life.[34] The important role that Earth's early minerals played in the prebiotic formation of peptides, proteins, and other biomolecules was revealed by understanding the adsorption behaviors and polymerization of amino acids on various ceramic surfaces.[35]

To date, chiral ceramic nanostructures with fascinating and unique properties triggered considerable interest and offered a range of potential nanotechnological applications. A large variety of metal and nonmetal oxides, nitrides, carbides, etc., with chiral geometries at the atomic, molecular, nano, meso, and micrometer scales have been demonstrated, including individual chiral ceramic NPs, mesoscale assemblies, and thin films.

Jinchen Fan received his Ph.D. degree from Shanghai Jiao Tong University in 2014. He is now an associate professor at Shanghai University of Electric Power, China. He joined Prof. Kotov's group as a visiting scholar from October 2017 to October 2019. His current research focus is on the fabrication of chiral nanoceramics and their applications in chiroptical activity and catalysis.

Nicholas A. Kotov pioneered conceptual foundations and technical realizations of biomimetic nanostructures, which include chiral nano-materials. Chiral ceramic nanostructures are being investigated in his laboratory for optical, magnetic, biological, and catalytic properties. His contribution to technology include nacre-mimetic nanocomposites including those from graphene oxide, 3D tissue replicas for drug-testing, chiral biosensors, and cartilage-like electrolytes for batteries. He is a founder of several start-up companies that commercialized bioinspired nanomaterials for biomedical, energy, and automotive technologies.

2. Synthetic Methods for Chiral Ceramic Nanostructures

2.1. Surface Modification

The chirality transfer from chiral organic molecules to individual NPs via surface modification provides a direct pathway to chiral nanoscale ceramics, which can be carried out by either during or after the formation of the nanostructures,[7,36] although the latter pathway is typically less effective.

Arrested growth in a chiral environment, is a common method for synthesis of chiral nanoceramics. In this context, individual chiral ceramic NPs from TiO_2,[37] tungsten oxide (WO_{3-x})[38] molybdenum oxide (MoO_{3-x}, MoO_2),[39] and zinc oxide (ZnO)[40] and Co_3O_4[22b] were reported. The atomic organization of ceramic NPs can be affected by chiral ligands inducing lattice distortion and crystal lattice displacement that may also be referred sometimes to as "chiral footprint."[41] The methods of density functional theory (DFT) calculations and molecular dynamics (MD) simulations were used to demonstrate the distortion and displacement and can detected by CD spectroscopy and Raman optical activity.[22b,38] Moreover, the lattice distortions and atomic displacements in the NP cores can be retained after removing the ligands. In addition, the coupling of the electronic states from chiral ligands to the surface states of the nanostructures can give rise to chiroptical bands with intensity comparable to those involving excitonic/plasmonic states in the inorganic core.[42]

2.2. Chiral Assemblies and Soft Templates

Most of organic amphiphiles can be assembled into chiral superstructures.[43] This series of superstructures can be used as soft templates in the preparation of helical ceramic nanomaterials including, SiO_2,[44] Ta_2O_5,[45] TiO_2,[46] ZrO_2,[47] and poly(bissilsesquioxane)[48] via the sol–gel transcription approach. Similarly, bio-macromolecules, such as peptides and DNA can serve as templates for realizing chiral ZnO[49] and silica structures.[50]

Chiral synthesis with sodium cholate (SC) also serves as a representative example of this method. Because of its amphiphilic character, SC self-assembles into a unique bilayer structure through the hydrogen bonding between hydroxyl groups.[51] Huang and co-workers[51b] used the SC assembled via coordination with calcium ions, well-defined helical nanoribbons for creating additional helical SiO_2 and ZnS by sol–gel process. Methods of chirality transfer from soft templates often include self-organization ceramic building blocks based on hydrogen bonding, van der Waals forces, π–π stacking, hydrophobic effect, electrostatic and Coulomb interactions, and metal coordination.[41] One of representative examples of chiral assembly is the preparation of chiral nanostructured silica that proceeds via

**ADVANCED
SCIENCE NEWS**

www.advancedsciencenews.com

**ADVANCED
MATERIALS**

www.advmat.de

nanoscale intermediated silica nanoparticles with a diameter of 20 to 400 nm depending on the conditions.[44,52] Various chiral silicas were synthesized via templating of silica precursors with chiral gelators, anionic and cationic surfactants, block polymers, and biomolecules. Chiral gelators can be assembled into supramolecular gels with different shapes, followed by chirality transfer to macroscale gels via condensation of nanoscale intermediates.[52b,53] The mirror asymmetry of nanostructured silicas manifests in chiroptical activity of supramolecular gels.

Benefiting from the supramolecular assembly of anionic and cationic surfactants, helical mesoporous silica also entered the field of chiral ceramic nanostructures.[44,52c,54] For anionic surfactants, most researchers believe that helical columnar model originated from a propeller-like micellar conformation.[55] The chirality could be controlled through the use of chiral surfactants and dopants to regulate the assembly conditions including temperature and pH. There remains controversy regarding the driving force for the chiral assembly of chiral silica with cationic surfactants; therefore, the chiral assembly behavior is worthy of further investigation.

2.3. Geometry Restricted Synthesis with Hard Templates

Chiral hard templates can be used as a straightforward method for the fabrication of chiral ceramic oxides. Using thick, thin, and coiled carbon nanofibers as templates, Ueda and co-workers[56] prepared helical ZrO_2, Al_2O_3, and SiO_2 ceramic fibers. In this process, the templates of carbon nanofibers were first coated with metal alkoxides by sol–gel polycondensation. The coated metal alkoxides were further changed into ceramic oxides by hydrolysis, and then the carbon nanofiber templates were removed by calcination. By casting a thin TiO_2 layer on chiral polypyrrole nanotubes (NTs) and carbon NTs, the chiral TiO_2 NTs with long-range chiral helical structures were obtained after removing the hard templates. Also, using carbon nanocoils as templates, helical metal oxide (Al_2O_3, SiO_2, TiO_2, HfO_2, and $ZnAl_2O_4$) NTs were realized by atomic layer deposition technology.[57] Chiral nematic nanocrystalline cellulose (NCC) films also play important role in synthesizing chiral ceramic oxides. MacLachlan first preserved the chiral nematic phase of nanocrystalline cellulose film by the air-drying method.[58] Using a hard template, the free-standing mesoporous silica films with long-range chiral nematic ordering were presented. Wang and co-workers[59] prepared the chiral nematic Eu^{3+}-doped ZrO_2 mesoporous films with Eu^{3+}-doped ZrO_2 by using nanocrystalline cellulose-templated chiral nematic mesoporous SiO_2 film as a template. The ability to efficiently remove the template and maintain acquired handedness remains a challenge and the focus of template-guided fabrication of chiral ceramic nanostructures.

2.4. Vapor Deposition

The process of vapor deposition, including chemical vapor deposition (CVD) and physical vapor deposition (PVD), has traditionally been the most common and direct method for creating chiral carbon nanomaterials, such as helical carbon nanotubes (CNTs), nanocoils, fibers, etc. Vapor deposition technology is also suitable for the growth of chiral ceramic solids.

As such, Wang and co-workers[60] prepared the helical ZnO nanohelices, nanosprings, and nanospirals in a solid–vapor growth process (**Figure 1**a–d). It was proposed that the formation of helices was thermodynamically and kinetically favored because the neighboring faces can achieve charge-neutrality and the neighboring loop can assist the growth of the crystal at its termini in a helix. Based on the solid–vapor growth method, such an electrostatic mechanism in the solid–vapor growth process, various helical and spring structured SiO_2,[61] SnO_2,[62] CuO,[63] $Ag_2V_4O_{11}$,[64] $Ag_{1.2}V_3O_8$,[65] $Na_2TiO_6O_{13}$,[66] $K_2Ti_6O_{13}$,[67] etc., micro or nanoceramic materials were prepared. Note however, that in these studies and many other studies in this section, the structures are obviously chiral, but the product is racemic. Both left and right helices and twisted ribbons are present there in equal amounts that precludes many albeit not all, practical applications of chiral structures.

Bae et al.[68] synthesized $ZnGa_2O_4$/ZnSe nanovines and $ZnGa_2O_4$ nanosprings by thermal evaporation using ZnSe nanowires (NWs). The lattice matching with the ZnSe NWs determined the growth direction of the helical $ZnGa_2O_4$ NWs. Subsequently, by means of electron tomography and high-resolution transmission electron microscopy (HRTEM), Kim et al.[69] found that the $ZnGa_2O_4$ nanosprings have four equivalent (011) growth directions. The zigzagged Zn_2SnO_4 NWs consisted of linked rhombohedrons having the side edges matched to the (110) direction and the (111) axial direction (Figure 1e,f).

2.5. Glancing Angle Deposition

Beside the wurtzite structural ceramic oxides, the universal way to control crystal growth with integrating glancing angle deposition (GLAD) in PVD process provided the solution and aroused researchers' interests. For this technique, the specific enantiomer of the chiral ceramic nanostructures can be obtained by varying the direction of the substrate rotation (**Figure 2**a).[70]

Robbie and Brett[71] first used GLAD to prepare porous films with helical columns of MgF_2 onto glass substrates. The helical columns of MgF_2 had 15 turns and a helical pitch of ≈350 nm.[71] Using the same method, they also prepared sculptured helical SiO and CaF films.[72] Adatom diffusion and atomic shadowing are the dominant growth mechanisms of GLAD. By taking advantage of macroscopic shadowing, spatially graded, helical nanostructured TiO_2 thin films were prepared by Brett and co-workers[73] The number of turns and pitches increased by the increase of deposition angles that ranged from 60° to 80°.

GLAD is widely adaptable to a variety of the synthesis spiral or helical metal oxide ceramic materials, such as TiO_2 (Figure 2b),[73] SiO_2 (Figure 2c),[74] ZrO_2 (Figure 2d),[75] WO_3 (Figure 2e),[76] HfO_2 (Figure 2f),[77] AlN (Figure 2g),[78] Ta_2O_5,[79] etc. Recently, GLAD technology has been used in the preparation of hybrid ceramic materials and heterostructure materials. Chueh and co-workers[80] designed a TiO_2–SiO_2
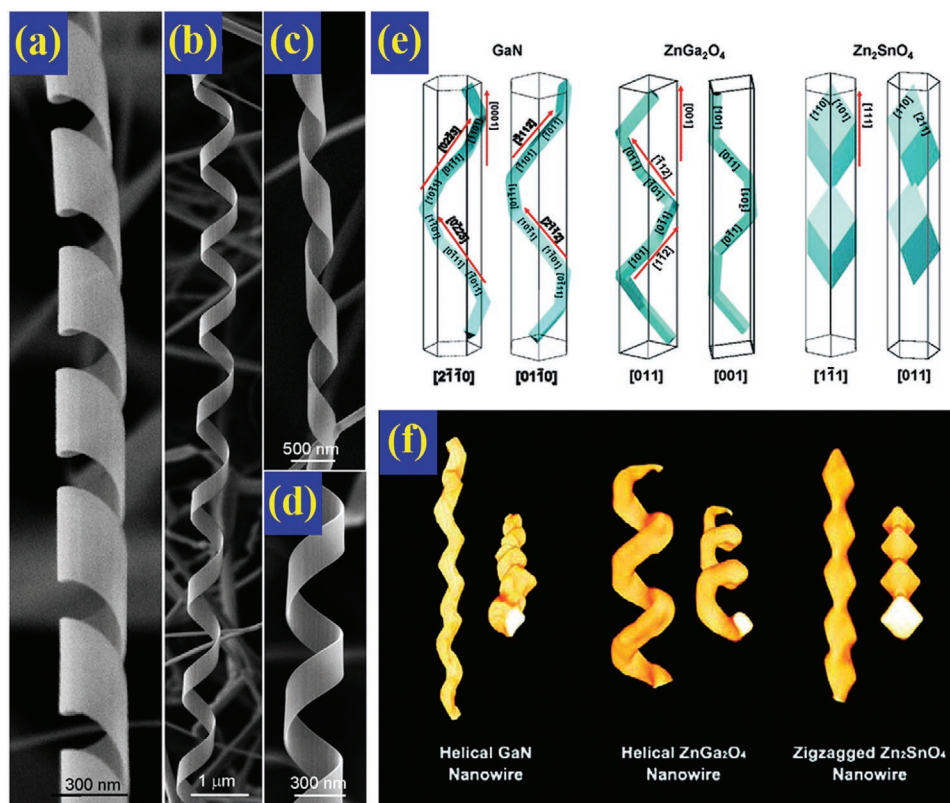
Figure 1. a–d) Typical SEM images of helical ZnO nanobelts. a–d) Reproduced with permission.[60a] Copyright 2005, American Association for the Advancement of Science. e) Schematic model constructed for helical GaN and $ZnGa_2O_4$ NWs and zigzagged Zn_2SnO_4 NWs. Reproduced with permission.[69] Copyright 2008, American Chemical Society. f) Images of the helical GaN $ZnGa_2O_4$ Zn_2SnO_4 NW obtained through tomographic 3D reconstruction. Reproduced with permission.[69] Copyright 2008, American Chemical Society.

core–shell nanostructure using GLAD. The TiO_2 helical nanostructures were first grown on a Cu(In,Ga)Se_2 device by the GLAD technique at an α of 80°, onto which a layer of SiO_2 was deposited (≈3.5 nm thick) using the Stöber method (Figure 2i). Karahan and Amine obtained their Si–Mo–O helices by the ion-assisted glancing angle electron beam co-evaporation of molybdenum oxide and silicon (Figure 2h).[81] With the help of magnetron sputtering, highly porous SnO_2 and Pd–SnO_2 films with different geometries were reported by Chundak et al.[82]

2.6. Hydrothermal and Solvothermal Methods

The term "hydrothermal process" was initially used in geology as a term to describe the natural process of water in the crust under the combined action of temperature and pressure. Today, hydrothermal and solvothermal methods have become an essential method of inorganic crystal synthetic chemistry. Perez-Pariente and co-workers[83] first prepared the beta zeolite from Na_2OTEA_2O–Al_2O_3–SiO_2–H_2O gel by the hydrothermal method and studied the crystallization mechanism. Newsam et al.[84]
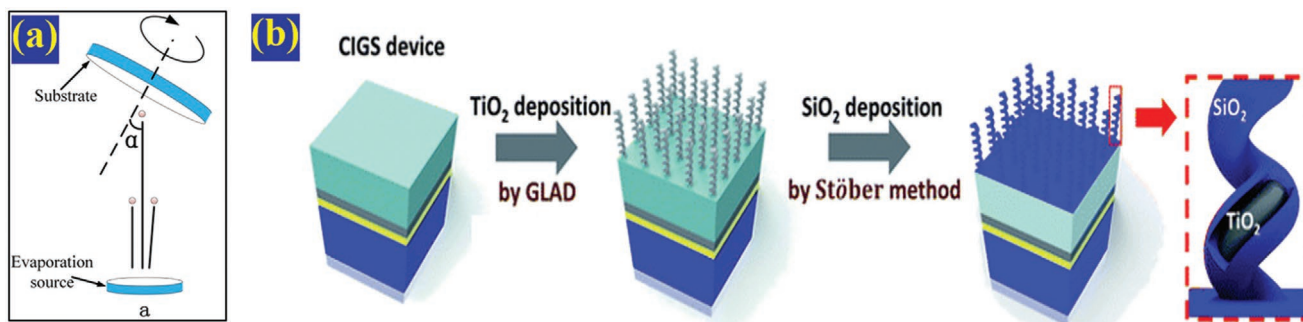
Figure 2. a) Schematic of the GLAD deposition. Reproduced with permission.[70d] Copyright 2015, Elsevier Ltd. b) Schematic diagram of preparing TiO_2–SiO_2 core–shell helical nanostructured coatings on Cu(In,Ga)Se_2. Reproduced with permission.[82] Copyright 2019, Royal Society of Chemistry.

ADVANCED
SCIENCE NEWS
www.advancedsciencenews.com

ADVANCED
MATERIALS
www.advmat.de

and Higgins et al.[85] independently determined the structure of zeolite beta and found that it is an intergrown hybrid of chiral polymorph A (P 4122 or P 4322) and achiral polymorph B (C$_2$/c).[86] Toward chiral polyoxometalates (POMs), Xu et al.[87] synthesized [NH$_3$(CH$_2$)$_2$NH$_2$(CH$_2$)$_2$NH$_3$]$_2$[Mo$_9$O$_{30}$] at 170 °C via hydrothermal techniques with polyamine. Inside the structures of the polymolybdate hybrid of [NH$_3$(CH$_2$)$_2$NH$_2$(CH$_2$)$_2$NH$_3$]$_2$-[Mo$_9$O$_{30}$], there are two symmetrically related helices with left-handed and right-handed enantiomorphs twisted in the centrosymmetric solid. In the formation process, the protonated amine NH$_3$(CH$_2$)$_2$NH$_2$(CH$_2$)$_2$NH$_3$]$^{3+}$ served as a charge compensation and structure-directing agent. With a deepened fundamental understanding of the crystallization for zeolite and polyoxometalate, structure-directing agents were considered to be very important for synthesizing final chiral structures.

Hydrothermal and solvothermal methods are also considered to be a convenient approach for synthesizing metal oxides. They provide a conversion pathway from chiral metal-organic assemblies to chiral metal oxide nanostructures. Duan et al.[88] reported the surfactant-mediated hydrothermal synthesis of well-defined, peony-like chiral CuO nanoflowers in the presence of symmetry breakers, (S)-(−)- or (R)-(+)-2-amino-3-phenyl-1-propanol (S)-(−)- or (R)-(+)-APP).

2.7. Screw-Dislocation-Driven Growth

As always with chiral molecular and nanoscale structures, it is not only necessary to grow chiral ceramic nanostructures, but also to break the symmetry in some way. Reviewing the classical Burton–Cabrera–Frank (BCF) theory for crystal growth, there are three dominant growth modes; dislocation-driven growth, layer-by-layer growth, and dendritic growth according to the driving force of supersaturation.[89] The dislocation-driven growth mechanism could be favored by intentional exploitation of low supersaturation conditions to allow the rational synthesis of 1D nanomaterials. The screw dislocation defects can provide self-perpetuating growth steps and break the symmetry of crystal growth.[21b]

In this respect, screw-dislocation-driven (SDD) growth method invoked a lot of interest in the preparation of chiral ceramic nanostructures with different dimensional morphologies. Screw dislocations have been shown to drive the growth of NWs, nanorods (NRs), and NTs (**Figure 3**a). Morin et al.[90] used SDD to grow 1D ZnO NWs and NTs from solution and explained the driving forces behind the formation of hollow tubes. The chirality is commonly caused by the elastic strain of the axial screw dislocation, which produces a corresponding Eshelby twist in the NW and NT. The Jin group synthesized Cu$_2$O NWs and NTs by reducing the cupric ions with various sugars. The growth of Cu$_2$O NWs and NTs has been demonstrated to be driven by screw dislocation resulting in the Eshelby twist.[91] Recently, Morin et al.[92] also studied the SDD growth of zinc hydroxy sulfate (ZHS). It was the first time that screw dislocations expanded to 2D ZHS nanoplates. The majority of ZHS nanoplates are hexagonal in shape with single or multiple dislocations with different handedness, and the cores located at the very center of the nanoplates (Figure 3b–e). The growth of 2D nanoplates of α-Co(OH)$_2$ and Ni(OH)$_2$ can also follow the dislocation-driven growth mechanism. As pointed out in Figure 3f, a model based on the differences between the velocities of steps at the core (V_c) and the outer edges of the dislocation hillocks (V_o) explained why or how one type of defect could lead to different morphologies.[92] In addition to synthetic routes of hydrolysis and solution redox, the routes of vapor deposition and thermal nitridation with dislocation-driven growth mechanism are also suitable for growing chiral ceramic structures.[89,90,93]

2.8. Chiral Biomineralization

Chiral biomineralized structures are commonly found in the natural world where organisms control the crystallization behavior of the inorganic minerals at the nanometer scale. Biomineralization processes are convenient in preparation of chiral ceramic nanostructures because they allow facile transfer of the molecular scale chirality from organic molecules to inorganic materials. Based on the process of biomimetic mineralization that is applicable to metals, semiconductor, and ceramic materials equally,[84] researchers have performed numerous trials to biomimetically synthesize chiral ceramics. As early as 2001, Orme et al.[94] found that the chiral amino acid, aspartic acid (Asp), can break the intrinsic symmetrical structure of a single calcium carbonate (calcite) crystal and endow it with a chiral shape. Observation of the behaviors of a series of chiral carboxylic acids (Asp, malic acid, and tartaric acid) on growing calcite crystals to obtain chiral morphologies, Kulp and Switzer[95] found the chiral sites that originated from chiral carboxylic acids have a critical impact on the final spiral orientation of calcite crystals.

In addition to amino acids, other biomolecules can induce chiral shapes in ceramic crystals. The helical fibrous calcite crystals with a chiral, twined spiral morphology were presented by Yamamoto and co-workers.[96] The directions of the helical fibrous CaCO$_3$ crystals were dependent on the chirality of the phosphoserine copolypeptides Ser(P)xAspy. Jiang et al.[97] found that the chiral acidic amino acids, Asp and glutamic acid, can change calcium carbonate phase formation in growth solution from calcite to vaterite (**Figure 4**a,b). With addition of Asp and glutamic acid (Glu), the predominantly vaterite was induced with highly complex supra structures and showed chiral orientations (Figure 4c–h). They proposed a growth model for the chiral calcium carbonate helicoids in terms of geometric orientations and relationships of vateritic NP subunits. In the model, the binding of the enantiomeric amino acid on the NP surfaces causes a change in their alignment with a tilt of −4° or +4° between neighboring prisms, and then generates platelet-edge curvature after amplification (Figure 4i).[97] To understand the chiral switching in biomineral superstructures induced by homochiral ʟ-amino acid, they subsequently found the chirality switching of calcium carbonate vaterite helicoid superstructures with ʟ-Asp and proposed a precise, four-step chiral switch mechanism.[98]

3. Versatile Chemistry of Chiral Ceramic Nanostructures

Structural control over chemical composition of chiral ceramic nanostructures is needed for optimizing chiroptical properties, asymmetric catalysis, chiral recognition, separation, etc. Here, we shall briefly summarize typical chiral ceramic structural

**ADVANCED
SCIENCE NEWS**

www.advancedsciencenews.com

**ADVANCED
MATERIALS**

www.advmat.de
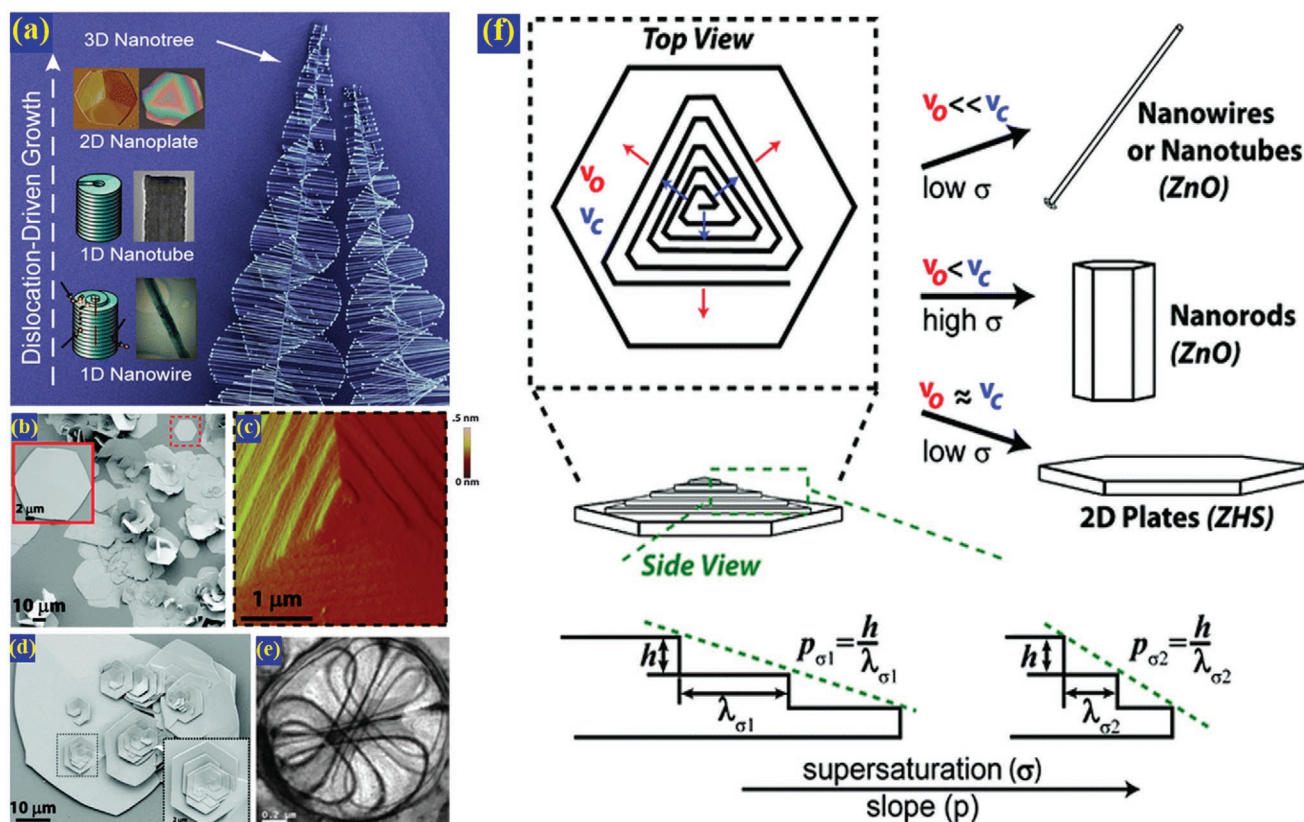
Figure 3. a) Overview of different dimensional nanomaterials obtained from SDD method. Reproduced with permission.[89] Copyright 2013, American Chemical Society. Characterization of screw dislocations in ZHS nanoplates: b) SEM image showing the hexagonal nanoplate. c) AFM image of the dislocation core and growth spirals. d) SEM image of a large nanoplate containing several screw dislocations with the growth spirals. e) Spider contours observed in the TEM image. f) Formation pathways for various nanomaterial morphologies driven by screw dislocations. b–f) Reproduced with permission.[92] Copyright 2011, American Chemical Society.

nanomaterials, including different chiral ceramic oxides, chiral polyoxometalates, and chiral zeolites. The emphasis will be made on the analyses of the mechanisms of chirality transfer which is critical for the future design of chiral ceramic materials.

3.1. Ceramic Oxides

Different ceramic oxides show different colors. From ancient times to the present, ceramic oxide, commonly used for ceramic glazes deposited on pottery, bring about a colorful world. In fact, almost all ceramic oxides can be chiral under some synthetic conditions. Naturally, different chiral ceramic oxides also produce different chiral structures and reveal related chemical, physical, and biological properties. Based on the current development of the field of chiral ceramic oxides, we shall discuss the conventional chiral nonmetal (silica) and metal oxide ceramic materials (zinc oxide, titanium oxide, cobalt oxide, tungsten, and molybdenum oxides).

3.1.1. Silicon Dioxide (SiO$_2$)

Since Mobil first reported the mesoporous MCM-41 (Mobil Composition of Matter No. 41), hierarchical mesoporous silicas

have attracted much attention owing to their uniform pore sizes, large specific surface areas, easy modification, etc.[20d,99] Chiral mesoporous silica contains a large number of chiral pores, which give rise to its selectivity and enantioselectivity, and is expected to be used in asymmetric catalysis.[44]

Chiral silica nanostructures, with different chiral structures and functionalities, constantly emerged through the design of various templates (gelators, surfactants, block polymers, and bio-macromolecules), control of the reaction parameters, and so on. As early as 1998, Shinkai and co-workers[100] accidentally discovered helical silica NTs while synthesizing silica materials using cholesterol-based organogelators as templates. The electrostatic interaction between anionic tetraethoxysilane (TEOS) oligomers and cationic cholesterol derivatives was proposed as the formation mechanism of tubular silica structure. Shimizu and co-workers[101] used sugar-based gelators, including double-helical fibers, to create templated double-helical silica NTs via transcription. They proposed a self-assembling model of the gelators; in this mode, gelators 1 and 2 formed a gel comprised of bilayered chiral fiber, which developed through intermolecular hydrogen-bonding and π–π stacking (**Figure 5**a,b). Oda et al.[102] studied the gelation assembly behaviors of the gemini surfactants cetyltrimethylammonium ions (C$_2$H$_4$-1,2-((CH$_3$)$_2$N$^+$C$_{16}$H$_{33}$)$_2$, CTA) with various counterions and found that the morphologies of the assembled aggregates was mainly
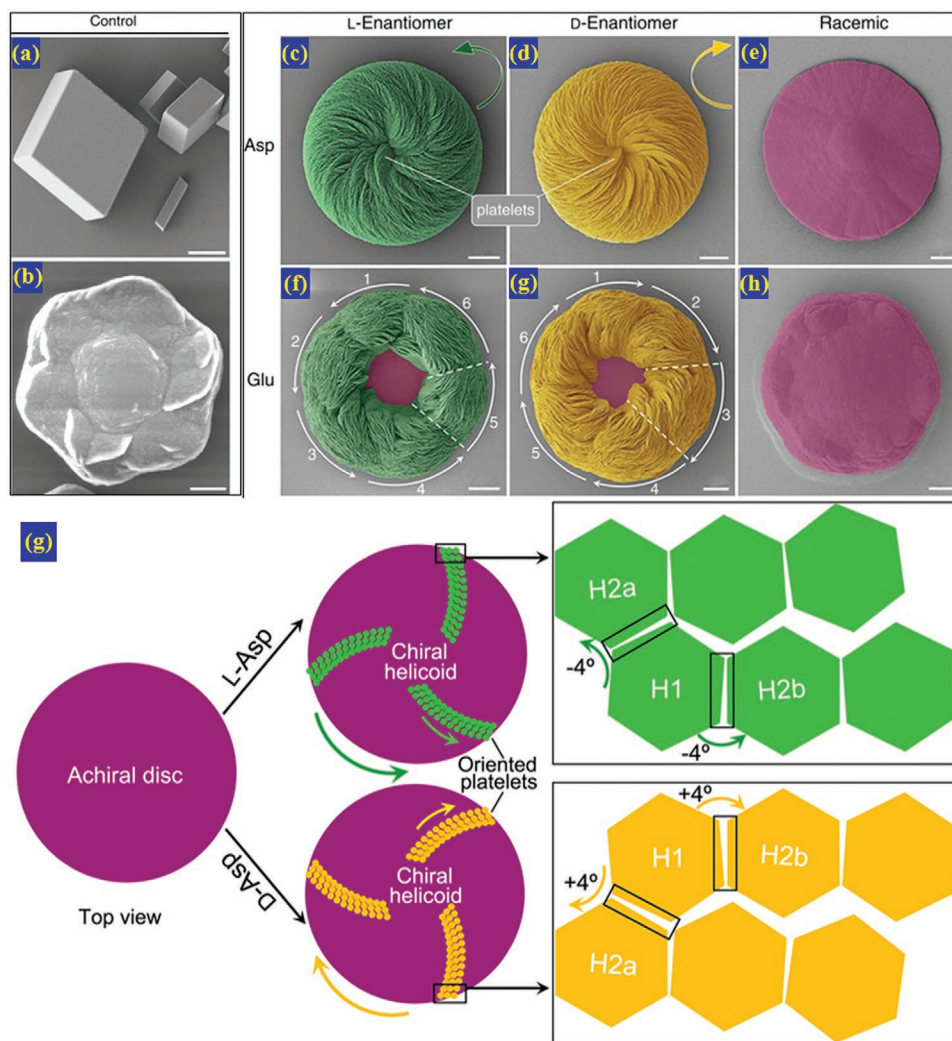
Figure 4. a,b) SEM images of rhombohedral calcite (a) and hexagonal vaterite (b) crystals. c–h) Pseudocolored SEM images of biomineralized vaterite structures grown in different enantiomers of Asp and Glu and their racemic mixtures. i) Schematic summary of the formation of hierarchically organized, chiral toroids. a–i) Reproduced under the terms of the CC-BY Creative Commons Attribution 4.0 International License (http://creativecommons.org/licenses/by/4.0/).[97] Copyright 2017, The Authors, published by Springer Nature.

determined by the covalent connections between the charged head groups as well as chiral centers in the counterions. Therefrom, the double helical silica fibrils were developed by sol–gel transcription of chiral aggregates of CTA with tartrate.[52f] The gelators assemblies of CTA with tartrate showed diverse chiral nanometric ribbons and tubules at different scales from nanometers to micrometers (Figure 5d).[103] Oda and co-workers[103] continuously found that the morphology of the silica helical nanostructures could be tuned by controlling parameters including temperature, concentration of reactants and aging times (Figure 5e). Afterwards, more and more gelator templates were developed and used for the preparation of chiral nanostructures.[104]

The use of surfactants opened the door for new routes to chiral mesoporous silica and its advanced applications. In 2004, Che et al. obtained chiral mesoporous silica with hexagonally ordered chiral channels based on co-assembly of chiral anionic surfactants and silica precursors.[52d] From TEM images, two different fringes can be observed in this chiral mesoporous silica and subsequently became a necessary proof of chiral channels (Figure 5d–g). Helical nanostructured silica could also be assembled from achiral anionic surfactants. For example, Che and co-workers[105] presented the chiral mesoporous silica NTs with helical channels by using achiral surfactant sodium dodecyl sulfate (SDS) and TMAPS as a template and co-structure-directing agent, respectively. In fact, the introduction of chiral dopants not only led to the change in structure from chiral mesoporous rods to chiral mesoporous hollow NTs but also was responsible for the enantiomeric excess of the products.[106]

Regarding the formation mechanism for chiral mesoporous silica templated by anionic surfactants, most researchers generally recognize the propeller micelle model (Figure 5c).[107] In the formation process, the internal conformational transformation of template molecules is more important than morphological transformation. Actually, cationic surfactants can
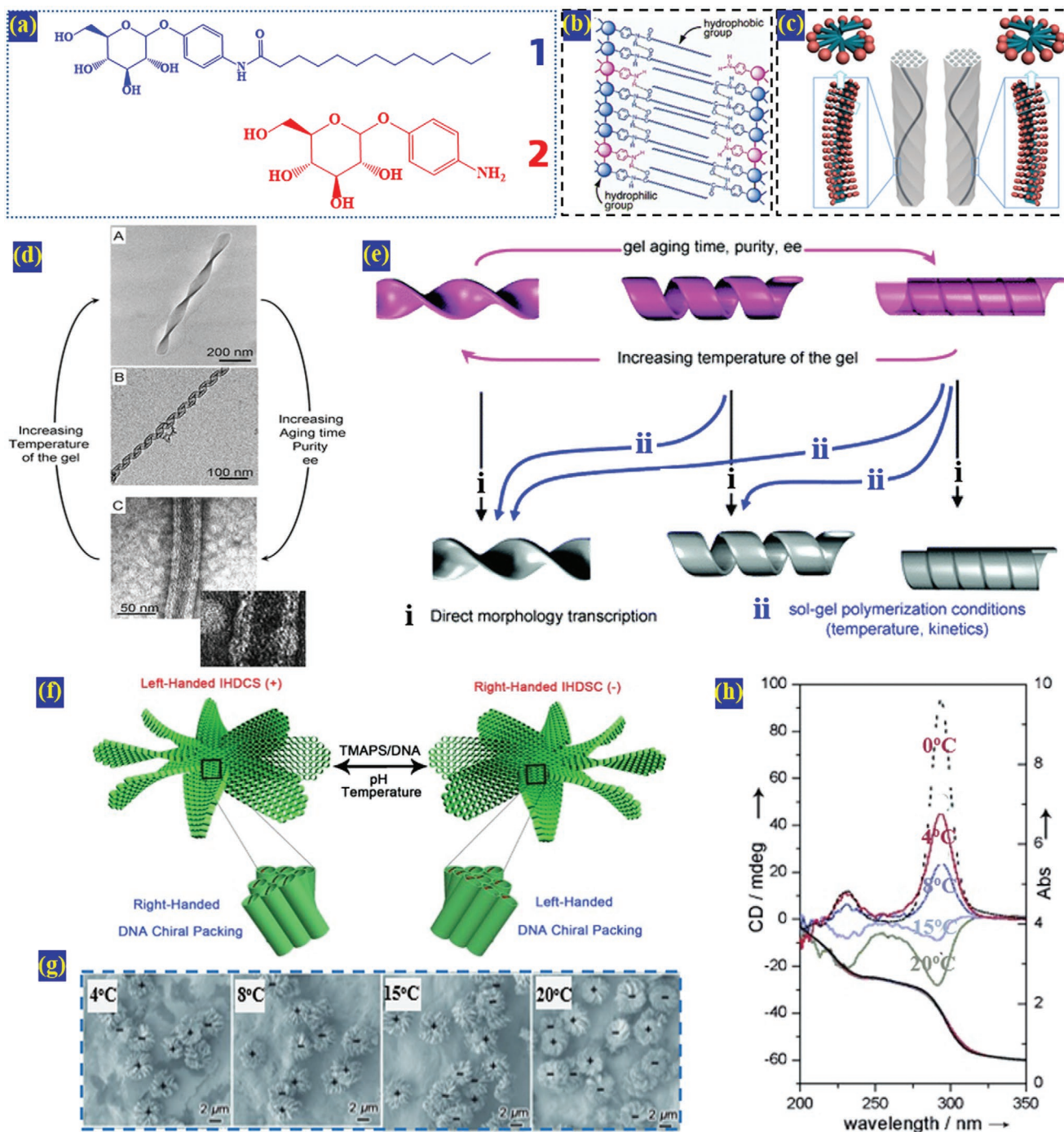
Figure 5. a) Chemical structures of gelators 1 and 2. b) A possible self-assembly model for bilayered chiral fiber. a,b) Reproduced with permission.[100] Copyright 2002, American Chemical Society. c) Molecular origin of chiral mesoporous silica derived from the helical packing of chiral amphiphiles. Reproduced with permission.[107] Copyright 2008, American Chemical Society. d) TEM images of twisted ribbon (A), helical ribbons (B). and tubules self-assembled from CTA with tartrate (C). d) Reproduced with permission.[103] Copyright 2008, American Chemical Society. e) Schematic representation of the diversity of inorganic silica chiral ribbons. Reproduced with permission.[103] Copyright 2008, American Chemical Society. f) Illustration of the macroscopic enantiomeric helical morphologies and corresponding opposite DNA chiral packing of impeller-like helical DNA–silica complexes. Reproduced with permission.[113] Copyright 2012, Wiley-VCH. g) SEM images for the IHDSCs obtained from different temperatures (left-handed: +; right-handed: –). Reproduced with permission.[113] Copyright 2012, Wiley-VCH. h) CD and UV–vis spectra for the IHDSCs obtained from different temperatures. Reproduced with permission.[113] Copyright 2012, Wiley-VCH.

**ADVANCED
SCIENCE NEWS**

www.advancedsciencenews.com

**ADVANCED
MATERIALS**

www.advmat.de

also be used for preparing chiral mesoporous silica, and their use was discovered before the use of anionic surfactants. A great deal of work has been published on chiral mesoporous silica including helix fibers and helix rods assembled from CTAB cationic surfactant. The co-use of different surfactants could also realize the construction of chiral mesoporous silica. Lin et al.[108] prepared different chiral mesoporous silica fibers with single-, double-, triple- and multi-helices by using ternary surfactant of alkyl trimethylammonium-dodecyl sulfate-Pluronic 123 (C_nTMAB-SDS-P_{123} ($n = 14$–18)). Different from the anionic surfactants, the formation mechanism based on CTAB cationic surfactant is still in dispute. Various models and theories, including "entropy-driven" model,[54b] topological defects,[109] "ice-like" water mode based on "entropy-driven,"[110] surface free energy reduction and energetic competition model,[111] etc., were proposed in order to understand the origin of chirality in helical mesostructured silica. Of course, biomolecules are mostly highly adaptable and ordered. Using the tetramer of folic acid as a template, Atluri et al.[112] presented the ordered mesoporous silicas (gyroid, chiral elongated, and spherical particles) with chiral hexagonal pore structures. Similarly to manychiral nanostructures from metal and semiconductors,[17] Liu et al.[113] employed DNA as a template and obtained enantiomeric impeller-like helical DNA–silica complexes. They found that the handedness of impeller-like helical DNA-silica complexes could be tuned by adjusting the temperature, pH, and the molar ratio of the quaternary ammonium phosphate group based on the interaction strength between the quaternary ammonium group of TMAPS and the phosphate of DNA (Figure 5h–j). In order to achieve chirality transfer at the supramolecular level, Qiu et al.[114] successfully demonstrated the chiral imprinting of chiral mesoporous silica is based on the chiral arrangement of poly(propiolic acid) sodium salt and tetraphenylporphine tetrasulfonic acid on quaternized chiral mesoporous silica through electrostatic interaction.

Despite the advancement of chiral ceramic nanostructures from silica, it remains a challenge to control their chiral geometry and the synthesis of specific desirable enantiomer instead of the randomly assembled structures. Increasing stirring rate[115] and reducing the concentration of ammonia solution will shorten the length of chiral silicas,[54b] while increasing the diameter and pitch. The pitch could also be increased with the ratio of alcohol to water.[116] The length of the organic carbon chain commonly determined the final length of silicas.[117] Factors including aging time, silicon precursors, ratio of co-surfactant to surfactant, acid–base ratio,[52c] catalyst concentration,[108] reaction temperature,[118] additive type, and dosage,[106] all affected the morphologies and structures of chiral silicas.

Toward chirality control, the transcription of chiral templates plays a key role in achieving the transition of chirality from the molecular level to mesoscopic level. For gelator-templated synthesis, the chirality is consistent with gelators, although it is difficult to get yields of pure enantiomers. Although the stereostructure of the template molecules, system temperature, acidity and alkalinity, and chiral dopant all affected the enantiomeric purity, high enantiomer excess and achieving homochiral silicas will remain a most challenging topic in the future.

3.1.2. Titanium Dioxide (TiO$_2$)

To some extent, the development of chiral TiO$_2$ has been influenced by chiral silica nanostructures. Like SiO$_2$, TiO$_2$ can also be produced from pyrolysis. The Shinkai group first used neutral dibenzo-30-crown-10-appended cholesterol gelator as a template to prepare helical TiO$_2$ ribbons and double-layered TiO$_2$ NTs followed by the studies of the Gun'ko and Kessler groups when they made TiO$_2$ NPs in presence of chiral surface ligand.[119] This mechanism is almost the same as that for cholesterol-based on gelator-templated chiral silicas. The metastable intermediate structures (linear ribbon, helical ribbon, and tubule) dominate the final chiral TiO$_2$ nanostructures.

More importantly, TiO$_2$ is a photosensitive material widely used in photocatalysis and solar cells. Anatase TiO$_2$ shows strong ultraviolet absorption in the range of wavelengths from 200 to 400 nm. For chiral TiO$_2$ with helical geometry, the optical chirality induced at the absorption bands is ubiquitous, owing to the electronic exciton coupling. To address the problem of the interaction in chiral transcription that originated from high hydrolysis rates of conventional TiO$_2$ sources, Che group used a titanium diisopropoxide bis(acetylacetonate) (TDA) to exploit the interaction between titanium species and a helical template of N-acyl-L-glutamic acid (C_n-L-Glu) amphiphile fibers, and finally obtained double-helical TiO$_2$ nanofibers (L-TiO$_2$-cal and D-TiO$_2$-cal) after calcination (**Figure 6**a–c).[120] The chirality of helical TiO$_2$ nanofibers was controlled by selectively using the lipid enantiomers, C_n-L-Glu or C_n-D-Glu. As seen in Figure 6d, the chiral lipid–TiO$_2$ hybrid (L-TiO$_2$-as and D-TiO$_2$-as) exhibited obvious strong mirror-image CD signals with a UV peak at ≈335 nm (Figure 6d). After calcination, the slight bathochromic shift indicates helical stacking of TiO$_2$ nanocrystals. Chiral TiO$_2$ nanofibers can, therefore, selectively reflect left- or right-handed circularly polarized light (CPL) in the UV absorption region. No exciton coupling was spectroscopically observed, which was associated with an overlapping manifold of electronic transitions.[120]

As mentioned above, owing to the high hydrolysis rates of conventional TiO$_2$ sources, successful preparation of chiral TiO$_2$ structures templated from a chiral soft template is rare. In contrast, the hard templates such as carbon nanofibers, carbon nanocoils, helical SiO$_2$, and chiral nematic nanocrystalline cellulose (NCC), etc. Recently, chiral TiO$_2$ nanofibers were prepared through the use of chiral polypyrrole NT (CPPyN) and chiral CNT (CCN) as hard templates. Chiral TiO$_2$ nanofibers exhibited the long-range chiral helical structure with the rotational misplaced arrangement anatase phase TiO$_2$ nanocrystals after the templates were removed. Chiral organization of TiO$_2$ nanocrystals gives rise to the electron-transition-based optical activity; in other words, the chiral TiO$_2$ nanofibers could selectively reflect left- and right-handed circularly polarized light.

Chiral TiO$_2$ nanostructures have bright prospects for nonlinear optics applications when made with enantioselective fashion.[121] MacLachlan and co-workers[122] created chiral mesoporous TiO$_2$ films with long-range nematic ordering by the use of a template of chiral nematic mesoporous silica templated from lyotropic chiral NCC. The chiral mesoporous TiO$_2$ films can selectively reflect left- and right-handed CPL owing to the chiral nematic organization of the titania crystallites. Besides the template-guided fabrication, Krause and Brett created a

**ADVANCED
SCIENCE NEWS**

www.advancedsciencenews.com

**ADVANCED
MATERIALS**

www.advmat.de
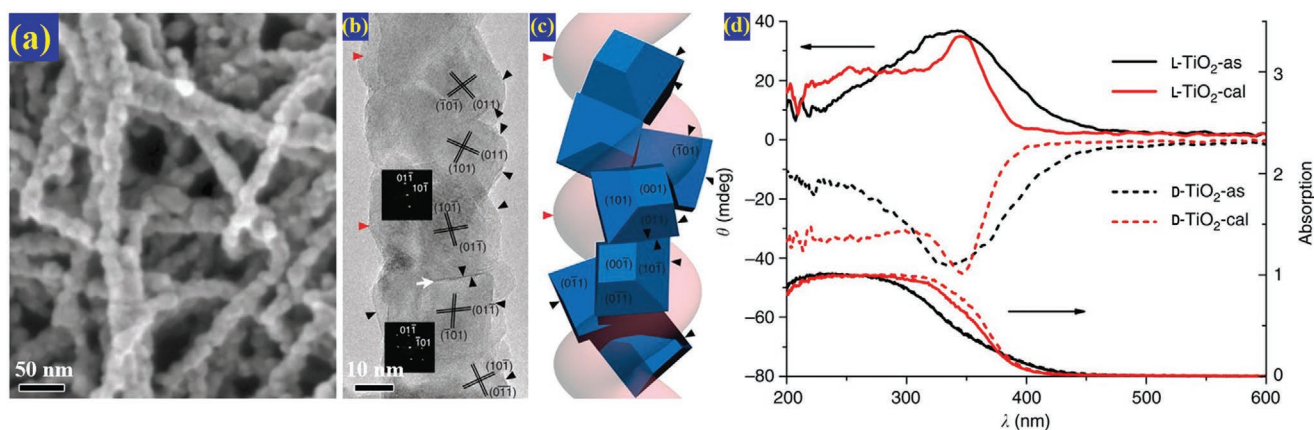
Figure 6. a) SEM image of the right-handed helical TiO$_2$ nanofibers. b) A HRTEM image and corresponding Fourier diffractograms of two TiO$_2$ nanocrystals. c) Structural model of helical stacking of anatase TiO$_2$ nanocrystals. d) UV–vis and CD spectra for chiral lipid–TiO$_2$ hybrid (L-TiO$_2$-as and D-TiO$_2$-as) and double-helical TiO$_2$ nanofiber (L-TiO$_2$-cal and D-TiO$_2$-cal). a–c) Reproduced with permission.[120] Copyright 2012, Springer Nature. d) Adapted with permission.[120] Copyright 2012, Springer Nature.

spatially graded transparent helical TiO$_2$ nanostructured film by virtue of GLAD technology. By changing the deposition angle, the circular birefringence of helical TiO$_2$ nanostructured film could be changed by introducing turns into the helical columnar structure. Most importantly, the graded helical TiO$_2$ nanostructured film shows polarization and frequency selectivity. By varying the spatial position of the incident light, the graded pitch inside of the film allows for frequency tuning. The helical structure brings strong polarization selectivity over a spatial range of 30 mm, together with tunability from the wavelength of 620 to 690 nm.[123] We have reason to believe chiral TiO$_2$ nanostructured films, as tunable circular polarizers, will find its place in photonic, spectral analysis, and sensing devices.[124]

3.1.3. Zinc Oxide

As an important and promising semiconductor, ZnO has been widely used in optoelectronic and piezoelectric fields. In 2001, by controlling the nucleation and growth with citrate ions, Liu and co-workers[125] prepared large arrays of oriented helical ZnO NRs and columns. During the process of ZnO growth, the citrate ions could strongly bond with Zn^{2+} ions through coordination, and then significantly inhibit the growth of the (002) surfaces of ZnO.

Wang and co-workers[126] reported in 2004 the controlled synthesis of single-crystal ZnO nanorings. Subsequently, the same group prepared the helical structure of ZnO with a solid–vapor growth process, using temperature to control growth kinetics (**Figure 7**a,b).[60a] As a wurtzite hexagonal ceramic oxide, ZnO, grown along the *c* axis, has two high energy polar surfaces, namely, the positively charged [0001]-Zn and negatively charged [0001]-O surfaces (Figure 7c,d).[60b] Because of this characteristic, the high energy polar surfaces induced a normal dipole moment and spontaneous polarization along the *c*-axis, as well as a divergence in surface energy. During the ZnO growth process, the spontaneous polarization and dipole moment induced electrostatic energy when the surface charges went uncompensated. To reduce the electrostatic energy, the ZnO nanobelt tends to roll up, which minimizes

or neutralizes the overall dipole moment. If the nanobelt is rolled uniradially, or loop-by-loop, the repulsive force between the charged surfaces stretches the nanohelix. Meanwhile, the elastic deformation force also pulls at the loops of the ZnO nanobelt. These mechanisms allow ZnO to grow into a group of chiral shaped nanohelices, nanosprings, and nanospirals (Figure 7e–h).[127] In summary, the balance of electrostatic interaction and the elastic deformation is the main reason for the final morphology of helical ZnO nanobelts.

A large number of synthesized helical ZnO nanostructures were formed by taking advantage of different zinc precursors made by the thermal evaporation method. With the help of Sb-induced thermal evaporation, Zhang and co-workers[128] prepared the superuniform helical ZnO, which has an axial direction of [0001], a perfect hexagonal cross-section, and length of tens of micrometers. Yu and co-workers[129] also obtained the helix-like ZnO nanostructure by thermal evaporation of zinc sulfide powder at 1020 °C. Until now, the application of chiral ZnO nanostructures were mainly focused on their mechanical properties, piezoelectricity, and polarization-induced ferroelectricity.[130] The helical ZnO nanobelt has been demonstrated to be highly elastic. However, the elasticity and piezoelectricity of chiral ZnO NTs is still in the theoretical research stage.[131]

Although great progress has been made in the fabrication of ZnO helical structures, there is still a lack of studies on chiral ZnO NPs and homochiral ZnO nanostructures. Very recently, Wei and co-workers[132] reported chiral ZnO NPs with ZnO cores capped with a chiral ligand of L-cysteine via an in situ functionalization. From the CD spectra, the minor peak at 324 nm demonstrated that the asymmetric structure of the ZnO core is induced by the L-cysteine chiral ligand. Because of their fluorescence quenching effect, the chiral ZnO NPs were used as probes for dopamine detection.

3.1.4. Copper Oxide (CuO)

The investigation of chiral CuO needs to start from the chiral CuO film first reported by Switzer et al.[133] The chiral CuO
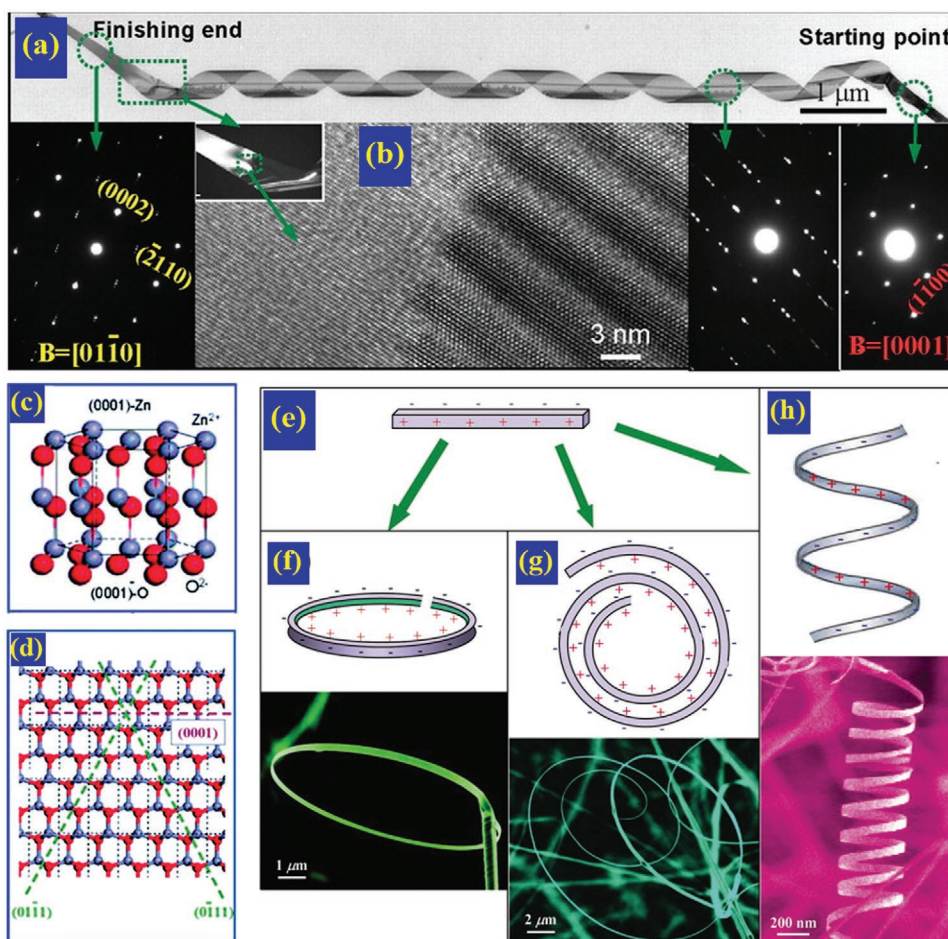
Figure 7. a) Low-magnification TEM image of a helical ZnO nanobelt with three typical SAED patterns of different regions. b) HRTEM image of a local area of the helical ZnO nanobelt. a,b) Reproduced with permission.[60a] Copyright 2005, American Association for the Advancement of Science. c,d) Wurtzite structure model of ZnO showing the ± (0001) polar surfaces. c,d) Reproduced with permission.[60b] Copyright 2004, Elsevier Ltd. e–h) Polar-surface-induced formation of nanorings, nanospirals, and nanohelices of ZnO and their formation processes. e–h) Reproduced with permission.[127c] Copyright 2004, Elsevier Ltd.

film was electrodeposited on a high-symmetry achiral surface of cubic Au (001) in the presence of tartrate ions. Like biomineralization, the chirality of the deposited CuO film can also be determined by chirality of the tartrate ions. The chiral CuO films deposited from Cu(II)(S,S)-tartrate and Cu(II)(R,R)-tartrate solutions show the [11$\bar{1}$] and [$\bar{1}$11] orientations, respectively. Notably, the chiral (S)-CuO film deposited from (S,S)-tartrate is more active for oxidizing (S,S)-tartrate and the (R)-CuO film is prone to the oxidation of the (R,R)-tartrate. Widmer et al.[134] further investigated chiral CuO films and established the [11$\bar{1}$] and [$\bar{1}$11] orientations. Moreover, the [11$\bar{1}$] and [$\bar{1}$11] orientations are non-superimposable mirror images and the [11$\bar{1}$] and [$\bar{1}$11] faces are enantiomorphs without a center of symmetry. Switzer et al.[133] also reported the epitaxial films of monoclinic CuO on single-crystal Cu (111). Notably, different from Au, the achiral Cu substrates are easily broken by the adsorption of chiral molecules with exposed chiral channels through the assembly.[135] The epitaxial electrodeposition is expected to be used increasingly in the synthesis of chiral ceramic oxide films.

Another compelling work on chiral CuO nanostructures involves CuO flower-like superstructures.[88] They reported the surfactant-mediated hydrothermal synthesis of chiral CuO assemblies in the presence of "symmetry-breakers" (S)-(−)- and (R)-(+)-2-amino-3-phenyl-1-propanol ((S)-(−)- and (R)-(+)-APP). During this process, the cupric ions (Cu^{2+}) served as a bridge, which linked the SDS and APP through electrostatic interaction and coordination bonding chelation, respectively (**Figure 8**a). The CuO shows 3D mesoscale structures assembled from many densely arranged nanoflakes grown from the singular center. The fan-shaped arrangement of nanoflakes rotated clockwise or counterclockwise (Figure 8b–g). The CD spectra of the chiral CuO assemblies exhibited a weak peak at ≈240 nm, a strong peak at ≈360 nm, and shoulders at ≈550 and ≈750 nm, which could be attributed to the helical stacking of the CuO NPs in close proximity (Figure 8h). Subsequently, the Chi group also deposited chiral CuO assemblies of nanoflakes on an activated quartz substrate and found that as-prepared chiral CuO films exhibit dual optical activities based on the electron transition absorption and reflection due to the hierarchical chirality.

**ADVANCED
SCIENCE NEWS**

www.advancedsciencenews.com

**ADVANCED
MATERIALS**

www.advmat.de
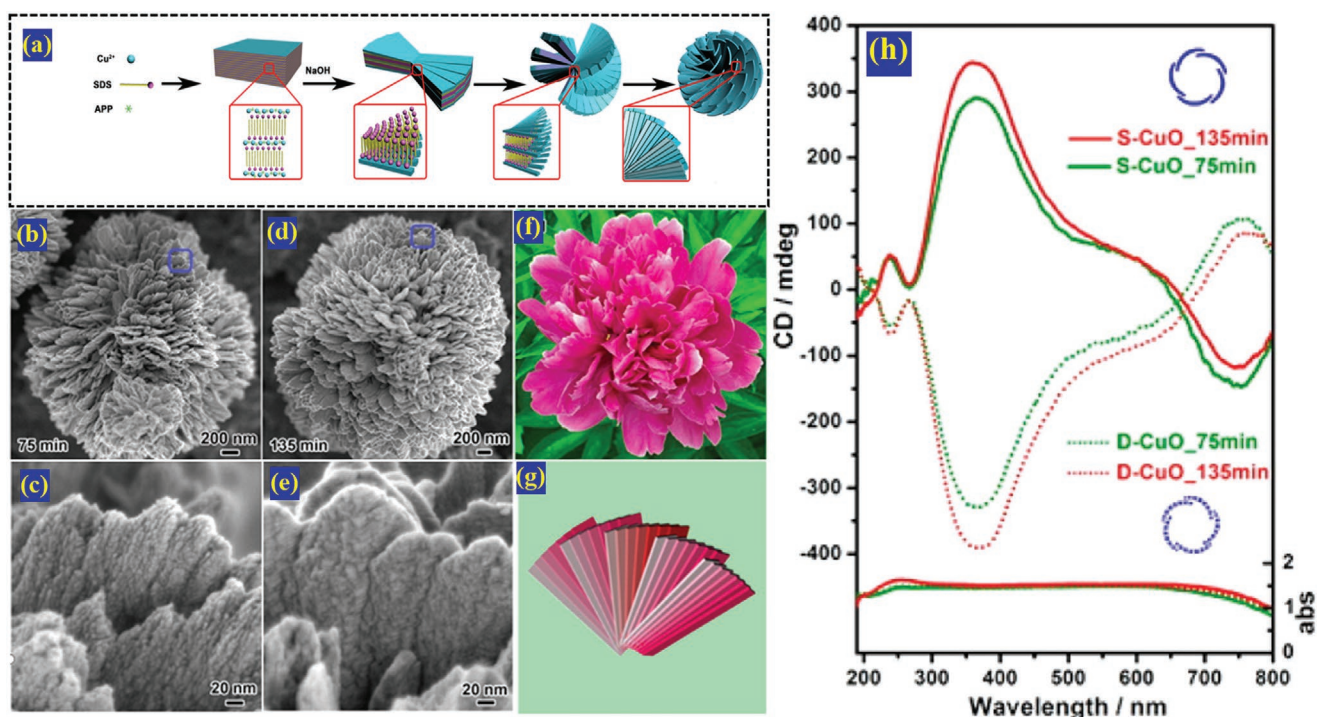
Figure 8. a) Schematic illustration for the preparation of a chiral CuO flower. SEM images and corresponding schematic drawings of sinistrorse CuO flower-like superstructures (*S*-CuO) synthesized with (*S*)–(–)–APP with different reaction times. b,d,f) Peony-like CuO flower-like superstructures with randomly stacked nanopetals. c,e,g) Nanoscale petals with helically arranged sub-nanopetals. h) Diffused reflection UV–vis absorption and CD spectra of the antipodal chiral CuO flower-like superstructures. a–h) Reproduced with permission.[88] Copyright 2014, American Chemical Society.

3.1.5. Tungsten (WO₃) and Molybdenum Oxides (MoO₃)

Tungsten and molybdenum oxides represent some of the most interesting materials used for the production of chiral nanostructures because of their strong optical and catalytic activity. Due to strong delocalization of charge carriers they can be have very strong chiroptical activity competing with that from semiconductor and metal chiral NPs. The chiral $WO_{3−x}$ NPs, with an average size of 1.6 ± 0.5 nm (**Figure 9**a), were prepared through surface functionalization of tungsten oxide hydrate ($WO_{3−x} \cdot H_2O$) using L- and D-enantiomers of Asp and proline (Pro). MD simulations revealed that the tungsten oxide lattice could be distorted by the incorporation of L- or D-Asp. The chiral $WO_{3−x}$ NPs capped with L- and D-Asp showed chiroptical activity over the entire spectral range of 200–1100 nm (Figure 9b). More importantly, the double-point binding of Asp to the tungsten oxide core with one additional C–O–W linkage brings NPs stronger distortion and CD signals than the single-point binding of Pro.[38]

Based on the research of chiral tungsten oxide ($WO_{3−x}$), Li et al.[39] presented novel chiral cysteine-capped molybdenum oxide ($MoO_{3−x}$) NPs and MoO_2 NPs with tunable absorption properties. The UV–vis absorption spectra reveal that the surface plasmonic peak and the metal-to-ligand charge–transfer (MLCT) peak could be tuned by altering the feed amounts of L- or D-cysteine ligands (Figure 9d). The $MoO_{3−x}$ NPs exhibit an energetic NIR absorption band induced by a surface plasmonic effect at ≈823 nm. Increasing the amount of L- or D-cysteine, the intensity of the plasmonic band decreases along with the

appearance of a weak absorption shoulder in the visible region. The transfer from plasmonic to MLCT band is attributed to the lower valence state of Mo in the NPs reduced by ligands. When the $MoO_{3−x}$ NPs were totally reduced to MoO_2 NPs, the plasmonic band disappeared entirely and was replaced by the influential MLCT band. More importantly, the chiral MoO_2 NPs show a prominent CD response with an ultrahigh *g*-factor value of ≈7 × 10⁻³ in the visible region owing to the strong Mo–S bond (Figure 9c).

3.2. Polyoxometalates

A POM is a polyatomic ion, usually an anion that consists of three or more transition metal oxyanions linked together by shared oxygen atoms to form closed 3D frameworks. Chiral POM-based ceramic frameworks generated tremendous and continuous research owing to their potential applications in asymmetric catalysis, chiral separations, etc.[136]

POMs with intrinsic chirality are rare, and most POM clusters are centro-symmetrical. It remains a challenging task to introduce chirality to POM-based materials. POMs are comprised of transition metals in high oxidation states (mainly V^V, Mo^{VI}, or W^{VI}) and oxo ligands.[137] Structurally, researchers tried to break the symmetry based on metal atoms and oxo ligands. Removing metal atoms in POM structures or replacing them with heterometals or other atoms can be used for preparing chiral POMs. Similarly, oxo ligand substitution with $M(CO)_3$ complexes (M = Mn or Re) or other

ADVANCED
SCIENCE NEWS

www.advancedsciencenews.com

ADVANCED
MATERIALS

www.advmat.de
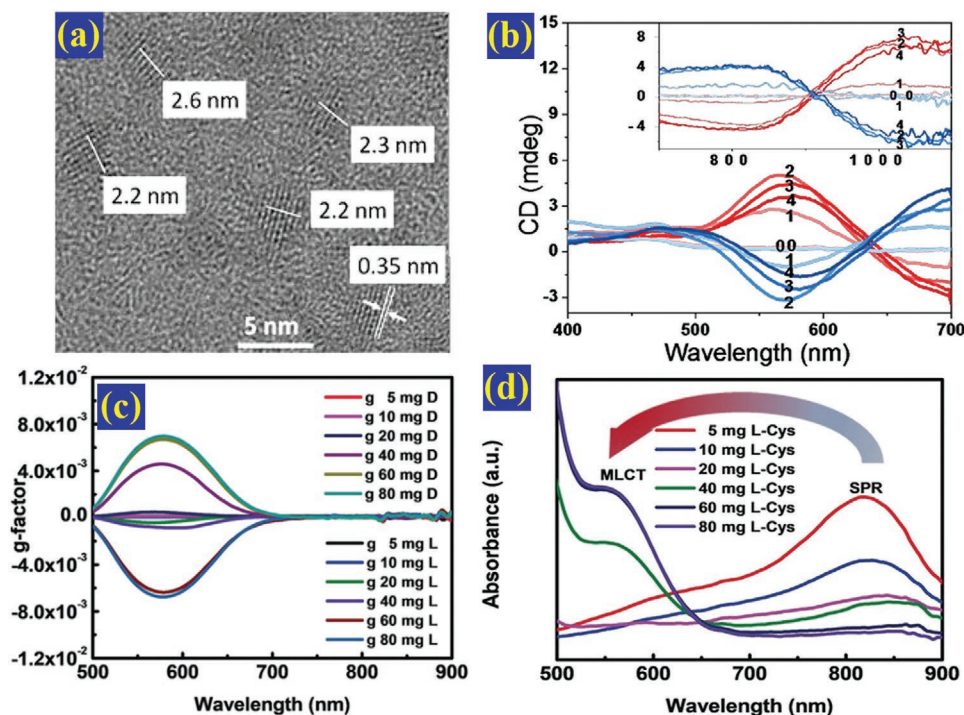
Figure 9. a) HRTEM image for L-Asp-capped WO$_{3-x}$ NPs. b) CD spectra of L-Asp-capped WO$_{3-x}$ NPs (red) and D-Asp-capped WO$_{3-x}$ NPs (blue) (inset: NIR range of corresponding CD spectra). c) g-Factor spectra of chiral molybdenum oxide NPs with different amounts of L- or D-cysteine. a–c) Reproduced with permission.[39] Copyright 2018, Wiley-VCH. d) Absorption spectra of L-cysteine-capped molybdenum oxide NPs. Reproduced with permission.[39] Copyright 2018, Wiley-VCH.

organic groups is also a way to create mirror image asymmetry in POMs.[138]

In comparison, it is easy to prepare chiral POMs by incorporating them with chiral organic ligands or chiral ligand–metal complexes into POM frameworks. Inoue and Yamase.[139] first found that the chiral lysine ligand could be coordinated to octamolybdate anions via carboxylate-O atoms at the vacant sites. Iijima et al.[140] obtained a chiral sandwich-type [Ln(α_2-P$_2$W$_{17}$O$_{61}$)$_2$]$^{17-}$ (Ln = La, Pr, Nd, Sm, Eu, Gd, Tb, Dy, Er, Tm, Yb, and Y) crystalline solid (**Figure 10**a) assembled from polyoxotungstates and chiral Pro through electrostatic interaction and packing effects (Figure 10b). They found that the competitive enantiomeric interactions between the L-/D-Pro and L-/D-polyanions could regulate the racemization of POMs.
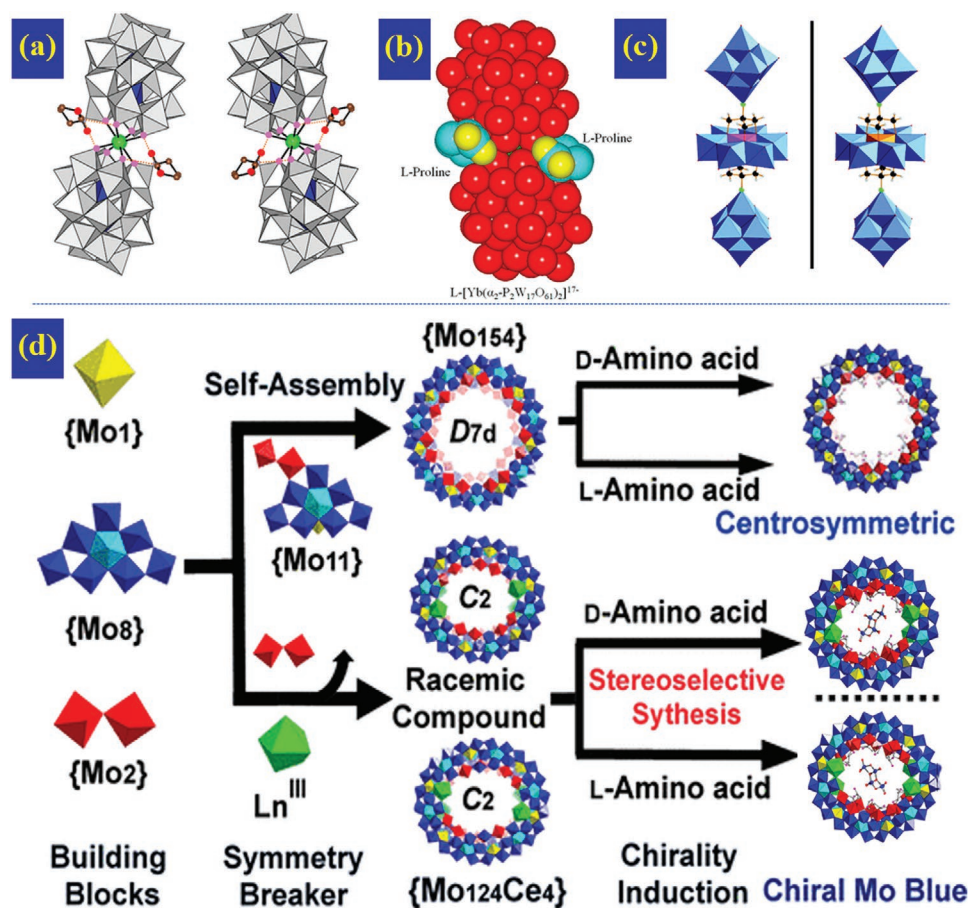
Theoretically, the approach of covalently bonding chiral ligands to POM anions is more conducive for transferring chirality to the entire POM framework. For instance, Cronin and co-workers reported chirality introduction through covalently bonded amino acids and peptides to Anderson-type polyoxomolybdates.[141] Very recently, through condensation of L-leucine methyl ester and Lindqvist-type hexavanadate, Wu and co-workers[142] reported a chiral POM hybrid and found the different enantiomers of supramolecular assemblies. Besides, chiral ligand–metal complexes can act as a "bridge" for chiral transfer. Wang and co-workers[143] employed the copper–Pro complex as a chirality director, and also prepared a chiral POM-based framework with homochiral intertwined double helices based on a Keggin cluster [BW$_{12}$O$_{40}$]$^{5-}$. The CD spectra revealed the chirality transfer from the chiral Pro ligand to the

copper–Pro complexes and, finally, to the POM-based framework through noncovalent bonding in the copper–Pro complexes. Fang et al.[144] also prepared enantiomerically pure, high-dimensional polytungstate frameworks with lacunary [P$_2$W$_{15}$O$_{56}$]$^{12-}$ ions assembled with chiral zirconium–tartrate coordination complex. Achiral ligands can also induce chirality to the whole POM frameworks with rational assembly. Conversely, the mechanism of chirality transfer mostly associated with the steric effect and conformation change. Wang and co-workers[145] found that the Cu$^+$ ions could link the achiral ligand of 1,1′-(1,4-butanediol)bis(imidazole), (bbi), with different conformations and generate chiral chains conformationally. Precisely two enantiomerically chiral [Cu^{II}Cu^{I}2(bbi)$_2$V$_{10}$O$_{26}$]$_\infty$ architectures have been prepared. The [V$_{10}$O$_{26}$]$^{4-}$ polyoxoanions are linked by two Cu^{II} ions via covalent bonding and two Cu^I ions through Cu–O interactions.

Additionally, the co-assembly of different POMs is also a common method used to form chiral POMs. Wei and co-workers[146] obtained the enantiopure chiral POM NRs, [Mo$_6$O$_{18}$NC(OCH$_2$)$_3$MMo$_6$O$_{18}$(OCH$_2$)$_3$CNMo$_6$O$_{18}$]$^{7-}$ (M = Mn^{III} or Fe^{III}), which are noncovalently assembled from two different achiral Lindqvist-type and Anderson-type POMs (Figure 10c). The obtained chiral POM NRs showed ferroelectric and nonlinear optical properties. Structurally, the bulky and heavy POMs hindered the free rotation of the C−N bond, which might be the origin of chirality.

In the past few decades, a series of helical organic–inorganic hybrids based on POM anions have been reported. Yang and co-workers[147] obtained three chiral POM–organic

1906738 (13 of 28)

**ADVANCED
SCIENCE NEWS**

www.advancedsciencenews.com

**ADVANCED
MATERIALS**

www.advmat.de

Figure 10. a) Combined polyhedral and ball-and-stick representation of two enantiomers of the $[Ln(\alpha_2-P_2W_{17}O_{61})_2]^{17-}$ polyanion (L-form; left; D-form; right). b) Space-filling model of the association composed of L-$[Yb(\alpha_2-P_2W_{17}O_{61})_2]^{17-}$ and two L-Pro molecules. a,b) Reproduced with permission.[140] Copyright 2018, American Chemical Society. c) Combined polyhedral and ball-and-stick representation of noncovalently assembled chiral rod-like molecular triads of $[Mo_6O_{18}NC(OCH_2)_3MMo_6O_{18}(OCH_2)_3CNMo_6O_{18}]^{7-}$, metals are Mn^{III} (left) and Fe^{III} (right). Reproduced with permission.[146] Copyright 2009, American Chemical Society. d) Stereoselective synthesis of chiral Mo blue POM clusters with "symmetry breaker." Reproduced with permission.[149] Copyright 2019, American Chemical Society.

frameworks from the chiral assembly of achiral species by employing $[Ni_6PW_9(H_2O)_6$ ($Ni_6 = [Ni_6(\mu_3\text{-OH})_3L_n]]^{9+}$, $PW_9 =$ B-α-$[PW_9O_{34}]^{9-}$and L = ethylenediamine or 1,2-diaminopropane) as secondary building units connected via rigid carboxylate linkers. The symmetry-breaking strategy is also known as an efficient way for the chiral assembly of POMs. Cronin's group reported a chiral polythioanion ring compound of $KH[NMe_4]_2[(Mo_2S_2O_2)_4(OH)_6(Mo_2O_8)(C_4O_4)]\cdot10H_2O$ assembled from achiral $[Mo_2S_2O_2(H_2O)_6]^{2+}$ fragments and $[Mo_2O_8]$ units. The appended $[Mo_2O_8]$ units acted as a "symmetry breaker" and broke the planarity of the ring.[148] Subsequently, they reported the stereoselective synthesis of a series of large chiral Mo Blue (MB) POM clusters by using lanthanides as "symmetry breakers" and different amino acids as chiral ligands (Figure 10d).[149]

3.3. Zeolites

Zeolites are crystalline microporous materials comprised of silicon, aluminum, and oxygen that form a corner-sharing tetrahedral framework. The unique porous structure of zeolites allows them to accommodate a wide variety of cations, such as Na$^+$, K$^+$, Ca^{2+}, Mg^{2+}, and others.[150] Because the pores of zeolites are about the same size as small molecules, zeolites are particularly well-suited for selective catalysis based on size and shape.

Perez-Pariente and co-workers[83] prepared the first zeolite beta from Na$_2$OTEA$_2$O–Al$_2$O$_3$–SiO$_2$–H$_2$O gel through the use of a hydrothermal method and studied the crystallization mechanism. Following this discovery, chiral zeolite research experienced tremendous development and their potential in enantioselective sorption, separation, and catalysis soon became apparent. Through a hydrothermal reaction, Soghomonian et al.[151] prepared an inorganic double-helix chiral vanadium phosphate, $[(CH_3)_2NH_2]K_4[V_{10}O_{10}(H_2O)_2(OH)_4(PO_4)_7]\cdot4H_2O$, which contains chiral double helices formed from interpenetrating spirals of vanadium oxo pentamers bonded together by P^{5+}. Sun et al.[152] obtained a germanosilicate mesoporous chiral zeolite with extra-large 30-ring windows following a crystallization process carried out at 175 °C. This material has a very open framework consisting of one unique cage $[4^26^4]$ and two
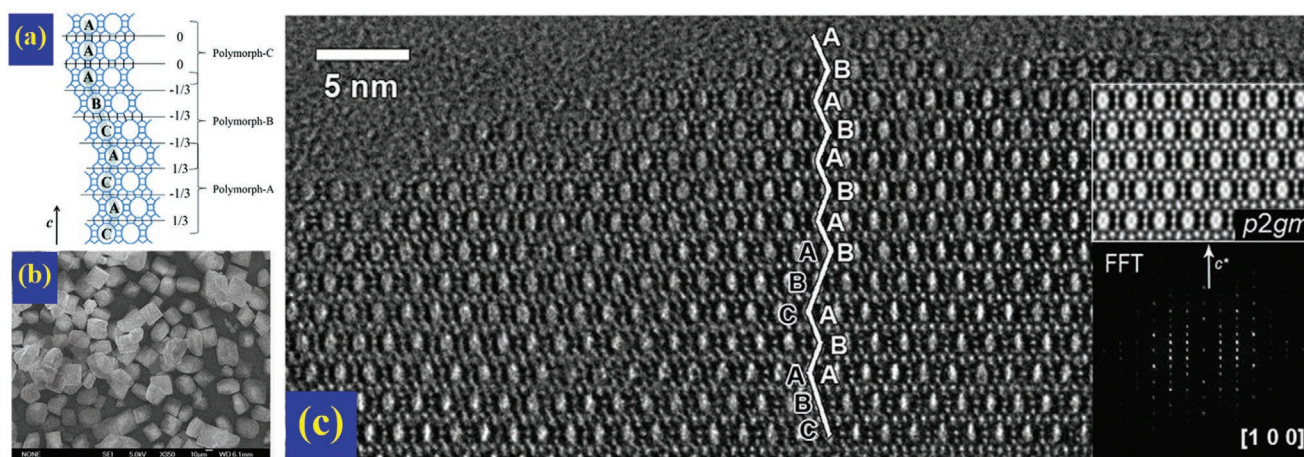
Figure 11. a) (010)-projection of intergrowth structure of β-zeolite. Reproduced with permission.[156] Copyright 2019, The Royal Society of Chemistry. The framework and corresponding nets of germanosilicate mesoporous chiral zeolite. b) SEM image of β-tetraethylammonium hydroxide. c) HRTEM image of the beta-tetraethylammonium hydroxide crystal. b,c) Reproduced under the terms of the CC-BY Creative Commons Attribution 4.0 International License (http://creativecommons.org/licenses/by/4.0/).[156] Copyright 2015, Springer Nature.

unique double 4 rings [4^6]; both are recurring motifs in zeolites (**Figure 11**b–d).

Among the currently known eight kinds of inherent chiral structures, including *BEA, CZP, GOO, -ITV, JRY, LTJ, OSO and STW, zeolite beta was the first chiral zeolite framework to be discovered and garnered the most research.[153] Zeolite beta is considered to be one of the most complex ceramic materials known. Briefly, there are three polymorphs A, B, and C, which intergrowth in zeolite beta (Figure 11a). Polymorph C_H, D, and E can be regarded as an ordered intergrowth by two of these three polymorphs (A, B, and C). Most of the synthetic zeolite betas only have two polymorphs (polymorph A and B).[31b,154]

As previously mentioned, polymorph A is chiral in the structures of zeolite. Synthesizing pure polymorph A is very challenging and hard to succeed. Davis and Lobo created a chiral zeolite beta by the introduction of chiral organic molecules to template polymorph A.[31a,155] Although there was not enough evidence to demonstrate the existence of pure polymorph A, the idea of using organic template molecules to control the synthesis of polymorph A is very significant in for the field of synthetic chiral zeolites. Over the next two decades, numerous different chiral and achiral organic structure-directing agents were used to synthesize chiral polymorph A enriched zeolite beta. Xu's group reported a generalized route for the synthesis of chiral polymorph A enriched zeolite beta using extremely concentrated fluoride media with five alkaline structure-directing agents, N,N-dimethyl-2,6-*cis*-dimethylpiperdinium hydroxide, N,N,N-trimethylcyclohexanaminium hydroxide, dimethyldiisopropylammonium hydroxide, N-ethyl-N,N-dimethylcyclohexanaminium hydroxide, and tetraethylammonium hydroxide. Consider, as an example, a β-tetraethylammonium hydroxide (TEAOH) crystal seen from a scanning electron microscopic (SEM) image (Figure 11e)—the bulk samples are uniform without impurities. HRTEM image for TEAOH with marked 12-MR channels revealed the dominance of polymorph A (Figure 11f).[156]

By controlling the hydrofluoric acid (HF) concentration (HF/OSDA >1.0), Zhang et al.[157] subsequently prepared a chiral polymorph-A enriched zeolite beta (55–65% A) in a high HF-concentrated medium with a variety of achiral OSDAs, including N-isobutyl-N-methylpyrrolidinium hydroxide, N-isopropyl-N-methylpyrrolidinium hydroxide, and N-isopentyl-N-methylpyrrolidinium hydroxide. Lu et al.[158] speculated that, for this reaction, the slow nucleation rate caused by the acidic medium might be an essential reason for the enrichment of chiral polymorph A in zeolite beta.

In general, increasing the proportion of polymorph A or enantiomerically pure polymorph A will remain the focus of research on chiral zeolite materials. Because the structure-directing agents are critical for controlling the pore dimensions and connectivity of synthetic zeolites, it could also serve as ligands inducing chirality. The design and synthesis of novel structure directing agents remains an important topic in the research field of chiral zeolites.[159]

4. Properties and Applications of Chiral Ceramic Nanostructures

4.1. Chiroptical Activity

With molecular, nano, and mesoscale geometry chiral inorganic nanostructures being the key determinant of chemical, physical, and biological properties, chiroptical activity is a secondary macroscopic property of chiral entities that arises from the way they interact with left and right circularly polarized light. Various chiral ceramic nanostructures show different optical activities, including optical rotation, circular dichroism, circularly polarized luminescence, Raman optical activity, and vibrational optical activity based on scattering, refraction or absorption.[160] The most often studied chiroptical property is CD, which reflects the differential interaction of the medium to the left and right circularly polarized light.[161] The optical activities of individual chiral ceramic NPs with semiconducting properties are mostly related to chirality of excitonic excited states. Some contribution to optical activity can be made from

**ADVANCED
SCIENCE NEWS**
www.advancedsciencenews.com

**ADVANCED
MATERIALS**
www.advmat.de

the quantum mechanical coupling of the chiral electronic states of the surface ligands with achiral excitons or surface states. Cleary et al.[37] prepared chiral TiO_2 NPs capped with chiral ligands of diphenylethylenediamine. With the ligand-induced effect, the original CD signals of organic ligands of (+) or (−)-diphenylethylenediamine between 256 and 268 nm disappeared, and were replaced by a broad peak, which begins at 350 nm. The optical activity originates from the overlapping of the highest occupied molecular orbital (HOMO) for the chiral ligand and the valence-band states for the TiO_2 NPs. Beyond the exciton coupling, once the core of a ceramic nanostructure is chiral, the excitonic states inevitably becomes chiral. As we mentioned in Section 3.1.5, the reported chiral $WO_{3−x}$ and $MoO_{3−x}$ NPs both exhibited strong optical activity, mostly due to the high distortion of their cores, which was induced by the interaction between ceramic NPs and chiral ligands. More importantly, the chiral $MoO_{3−x}$ NPs exhibited tunable chiroptical properties from the plasmonic band to the MLCT band owing to valence change from Mo^{VI} to Mo^{IV}. Most ceramic nanostructures exhibit electronic transitions in UV or visible range. To endow chirality in true ceramic nanostructures, Liu et al.[120] prepared the chiral TiO_2 nanofibers by calcination of the helical antipodal lipid–TiO_2 hybrids assembled C_{18}-L/D-Glu lipid enantiomers. The chiral TiO_2 nanofibers were organized by the stacks of small anatase TiO_2 crystals and showed electron transition-based optical activity. Diversified synthetic methods provide the basis for hierarchical chiral ceramic nanostructures with fascinating optical properties. With L- or D-methionine inducing self-assembly, the chiral ZnO films exhibited unique hierarchical nanostructures that ranged from atomic to micrometer scale. Surprisingly, the hierarchical chiral ZnO film simultaneously showed prominent electron transition and scattering-based optical activities, circularly polarized luminescence, and Raman optical activity (ROA), which originated from the different chiral scales.[162]

Based on recent progress, polarization modulation enabled by chiral inorganic nanostructures has become an intense research direction. Previously, the chiral ceramic oxide films we mentioned could show polarization and frequency selectivity. Additionally, chiral ceramic nanostructures are also expected to have distinct circularly polarized photoluminescence. Different properties of various ceramic oxides could give rise to interesting and unique applications for chiral ceramic nanostructures. Chiral Co_3O_4 NPs is a significant example in this perspective due to its magnetism. Chiral Co_3O_4 NPs can be prepared with average sizes of ≈5 nm using L- and D-cysteine as surface ligands. The chiral Co_3O_4 NPs exhibited chiroptical activity in the visible range with anisotropy g-factors as high as 0.02, which is nearly ten times higher than those of nonmagnetic NPs of comparable size (**Figure 12**a,b). Based on chirality transfer, the interaction between the L- or D-cysteine chiral ligand and the Co_3O_4 core induced the crystal lattice distortions, which can be confidently identified by ROA spectra and scanning tunneling electron microscopy (STEM) images. To better understand the nature of the chirality transfer in the Co_3O_4 ceramic cores, computational study of atomic-scale MD simulations were performed. The distortion of Co_3O_4 lattice can be visualized by MD simulations to reveal the mechanism of chirality transfer from the surface ligands to the ceramic core. More importantly, the combination

of chirality and magnetic properties opened up new horizons for real-time modulation of chiroptical activity. Chiral Co_3O_4 NPs were encapsulated into a transparent polyacrylamide (PAM) gel so as to avoid optical variation that arise from the movements of NPs. By modulating magnetic fields, the transparency of the chiral Co_3O_4 NP gels to circularly polarized light beams in the ultraviolet range could be reversibly altered due to the rapid alignment of magnetic moments of cobalt atoms (Figure 12c).[22b]

4.2. Mechanical Properties

Studies of the mechanical properties of chiral ceramic nanomaterials are mainly focused on the helical ceramic nanostructures. Like macroscopic springs, the helical ceramic nanostructures can undergo elastic deformation and return to their original structure. However, the nanoscale helices are too small to be directly observed, manipulated, or measured like macroscopic specimen samples.[163] Thus, in situ manipulators have been developed using optical microscopy, atomic force microscopy (AFM), SEM, and TEM to directly position, manipulate, and measure the mechanical properties of nanohelices. Using a tip-cantilever assembly attached to a conventional AFM, Liu et al.[164] studied the mechanics of patterned helical Si springs on a Si substrate. Toward the ZnO nanohelices, Wang and co-workers[60a] used AFM and FIB to manipulate a nanohelix and found that ZnO nanohelices have a rigid structure (**Figure 13**a). After cutting, the segments of ZnO nanohelices can be preserved without visible relaxation. Measuring by AFM with use of the force–displacement (F–Z) curve, the transverse spring constant of the nanohelix was 3.9, 4.6, 4.5, and 5.3 N $m^{−1}$ for one to four turns, respectively. After conversion, the corresponding elastic moduli of the nanohelix are 42, 49, 48, and 57 GPa for the four turns, respectively (Figure 13b,c). To further study the elastic property of ZnO nanohelix, Wang's group used continuous in situ stretching and compression in SEM and AFM and found a superelasticity (shape memory) behavior in superlattice-structured ZnO nanohelices. The spring constant of the helices can be increased to 300–800% of the initial value.[130b] Similarly, Qin et al.[57] studied the moduli of the helical Al_2O_3 NTs by atomic layer deposition with carbon nanocoils as templates (Figure 13d). By pushing the NTs at the midpoint with calibrated Si cantilevers, the moduli of the helical and straight Al_2O_3 NTs are 30.1 and 112.0 GPa, respectively, as determined from force–deflection (F–D) curves by manipulating the AFM tips (Figure 13e–h). The modulus of the helical NTs is nearly four times smaller than that of the straight NTs, which indicates that the helical NTs are much more flexible because of their geometry.[57]

4.3. Catalysis

Early studies showed that the surface immobilization of amino acids on the ceramic surfaces facilitates the condensation reaction.[165] Generally, the physicochemical properties of ceramic nanostructures have made chiral ceramic materials widely used in electrocatalysis, photocatalysis and enantioselective catalysis, etc.
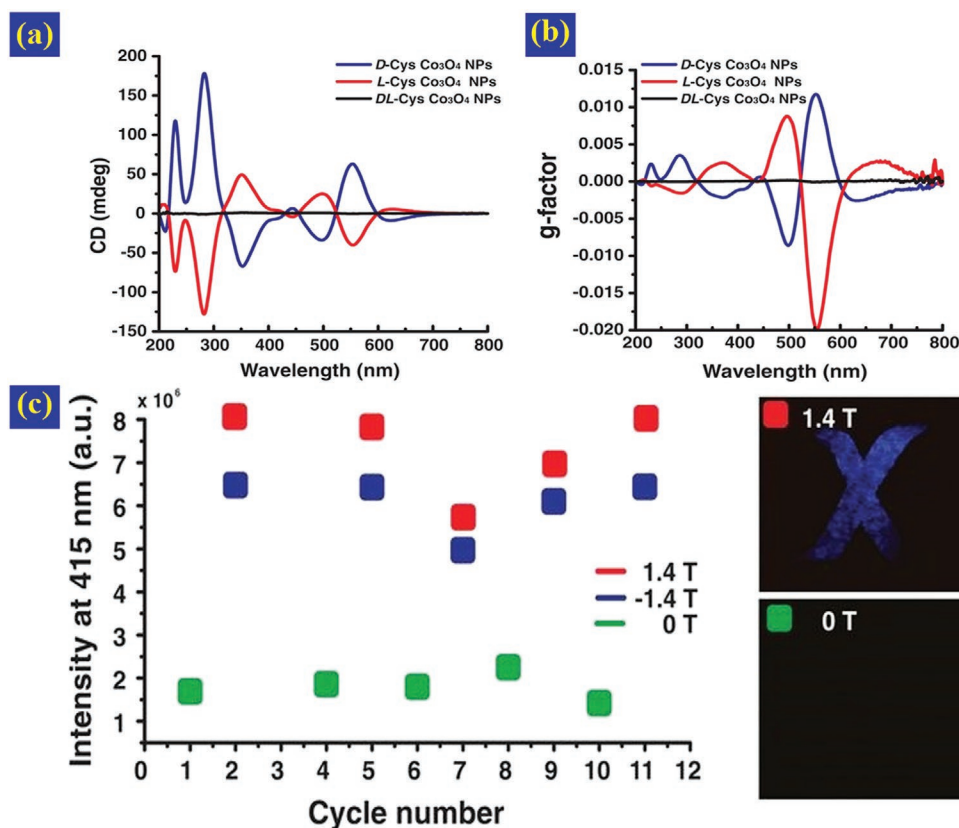
Figure 12. a) CD spectra and b) *g*-factor of synthesized chiral Co_3O_4 NPs. c) Cycling profile of emission intensity at 415 nm of gels with and without magnetic fields and corresponding photographs of blue-emitting light from fluorescent paper. a–c) Reproduced with permission.[22b] Copyright 2018, The Authors, published by American Association for the Advancement of Science.

Ghosh et al.[166] hypothesized that the chiral CuO films could act as electron spin filters and exhibit high selectivity toward oxygen reduction reactions (ORR). Due to the electron spin dependence for the ORR and the generation of spin-polarized reaction intermediates, the chiral CuO film-based anodes enable selective production of O_2 over H_2O_2 (**Figure 14**a). The surface plasmon resonance (SPR) can alter the chiral signals over the whole visible and near-IR range, which can dramatically amplify the light absorption and, therefore, be employed to produce high photocatalytic performances. Therefore, many investigations were made based on the hybrids of plasmonic metal NPs and chiral ceramic nanostructures. Wang et al.[167] prepared the plasmonic Ag/AgCl@helical TiO_2 nanofibers photocatalyst. Because the chiral structure of the TiO_2 nanofibers boost the SPR effect of the supported Ag/AgCl materials, the Ag/AgCl@ helical TiO_2 nanofibers show higher 17-*b*-ethinylestradiol degradation rates than those of chiral TiO_2 nanofibers under visible light irradiation. As a quantum optical–electrical phenomenon confined to metal surfaces, the SPR frequency can be tuned by altering the size and shape of noble metal NPs, which can dramatically amplify the visible light absorption. Zhang et al.[168] deposited the Ag NPs onto the surfaces of chiral TiO_2 for photodegradation and found that the size of Ag NPs affects the photocatalytic activity under visible-light irradiation, and the optimal size of Ag NPs was determined to be 12–14 nm. Introduction of the helical structure can significantly improve the

optical absorption and energy bandgap. Zheng et al.[169] synthesized the helical C_3N_4 NRs by using a chiral mesoporous silica template. Compared to bulk C_3N_4, the helical C_3N_4 NRs have a higher bandgap energy of ≈2.75 eV and show an improved light-harvesting capability across the whole optical spectrum, especially at wavelengths exceeding 420 nm. The helical C_3N_4 NRs have been shown to demonstrate photocatalytic capability towards hydrogen evolution, water oxidation, and CO_2-to-CO conversion.

In addition to electrocatalysis and photocatalysis, enantioselective catalysis has been one of the key research topics in chiral nanostructures. Chiral ceramic nanostructures for enantioselective catalysis should have nonracemic chiral surface features at the length scale of molecules. Chiral salen–metal complexes,[170] chiral hydrogen-bond donors,[171] chiral metal–organic assemblies,[172] chiral coordination polymers,[173] and different chiral ligands (C_2-symmetric ligands, N-heterocyclic carbenes, chiral ferrocene, and P-chiral phosphorus ligands, etc.) are widely used for asymmetric catalysis.[174] In the early 2000s, Soai and co-workers[175] found that chiral helical silica can induce the asymmetric synthesis of chiral pyrimidyl alkanol. Due to the strong Lewis and Brønsted acidity, chiral POM-based materials have been commonly used as enantioselective catalysts.[137a,176] The outstanding developments in this area were reported by Luo and co-workers, who developed a noncovalent immobilization
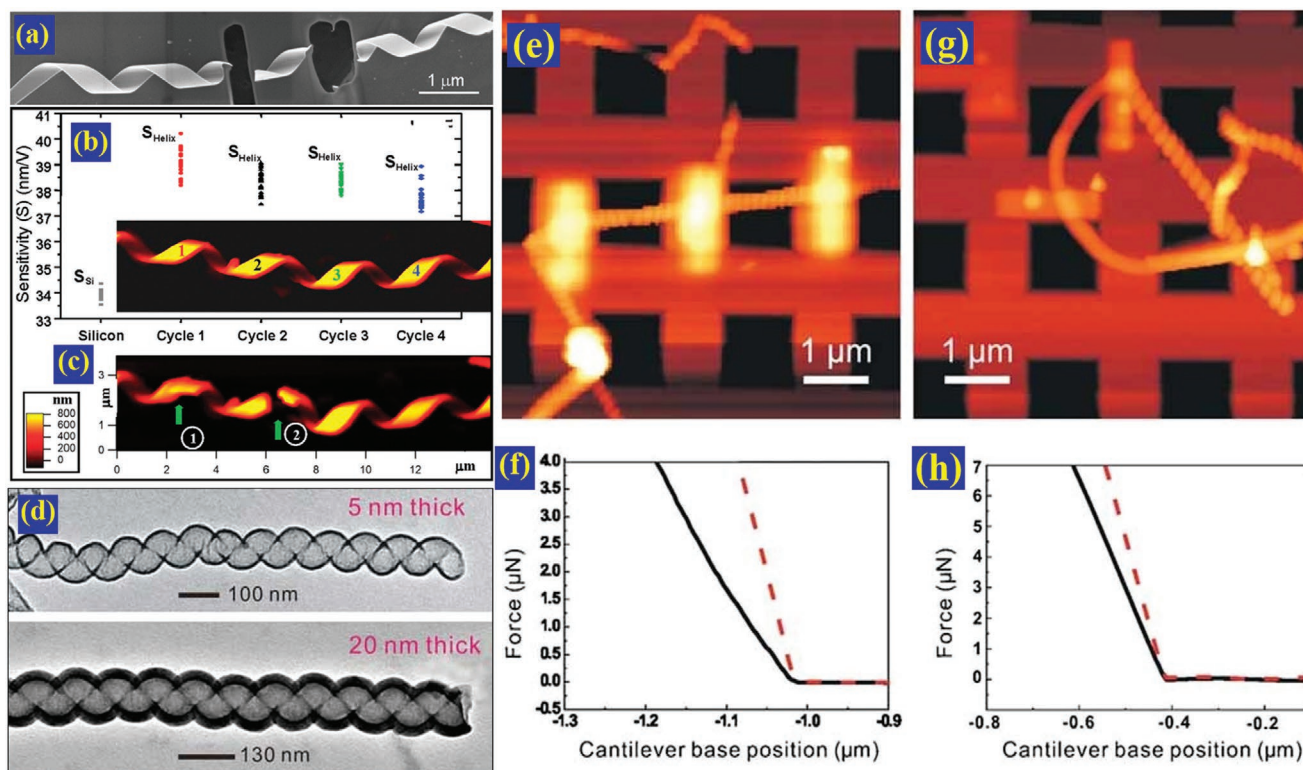
Figure 13. a) SEM image of an FIB-cut ZnO nanohelix with shape preservation. b) AFM contact-mode measurement of the sensitivity of the photodetector for the silicon substrate and the four turns of a ZnO nanohelix. c) Fracture of the nanohelix at two consecutive turns by the AFM tip, showing preservation of helical shape in the sectioned region. a–c) Reproduced with permission.[60a] Copyright 2005, American Association for the Advancement of Science. d) TEM images of helical NTs with different thicknesses. e) AFM image and f) F–D curves of a helical Al_2O_3 NT with an outer diameter of 123 nm. g) AFM image and h) F–D curves of a helical NT with an outer diameter of 131 nm. d–h) Reproduced with permission.[57] Copyright 2010, Wiley-VCH.
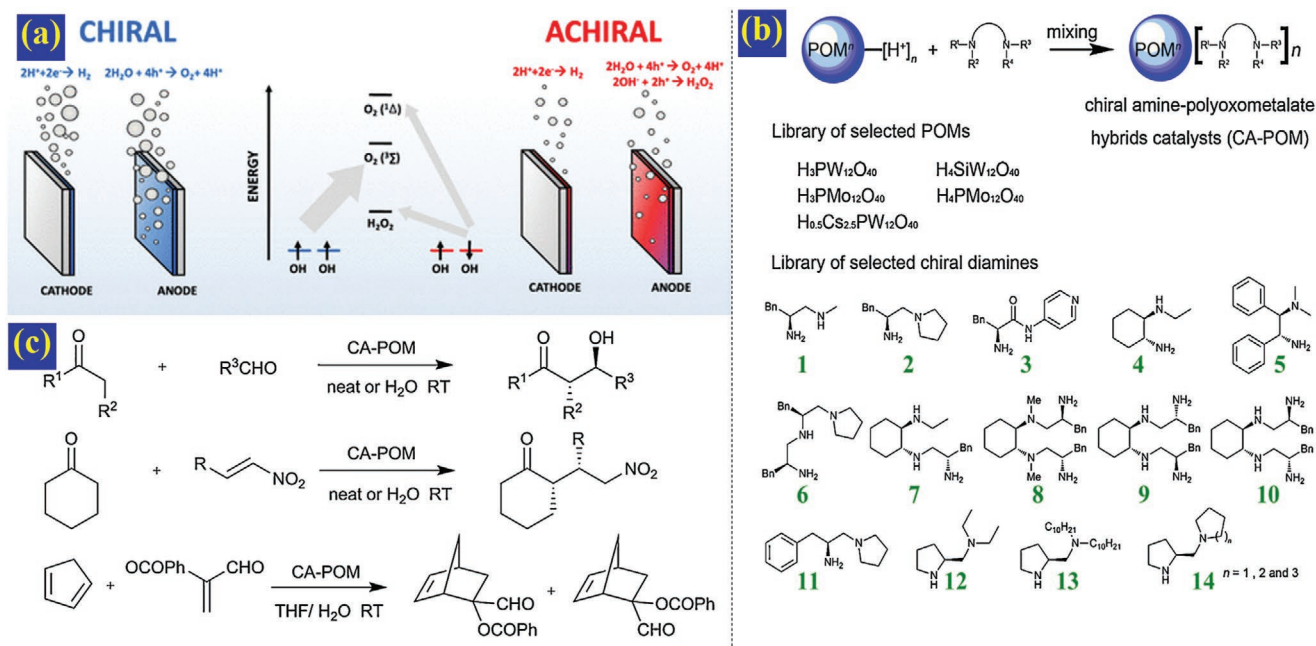
Figure 14. a) Schematic illustration for comparison of chiral and achiral CuO films as ORR electrocatalysts. Reproduced with permission.[166] Copyright 2019, American Chemical Society. b) Strategy for the construction of CA-POM hybrid catalysts. c) CA-POM hybrids catalyzed direct aldol, Michael addition, and Diels–Alder reactions. b,c) Reproduced with permission.[137a] Copyright 2013, Elsevier B.V.

**ADVANCED
SCIENCE NEWS**

www.advancedsciencenews.com

**ADVANCED
MATERIALS**

www.advmat.de

strategy by utilizing multidentate chiral amines and POMs (Figure 14b).[177] The chiral CA-POM catalysts afforded the desired products with high yields and enantioselectivities for aldol reactions between simple ketones and aromatic aldehydes, the Michael addition of cyclohexanone to nitroalkene, and the Diels–Alder cycloaddition of α-substituted acroleins under either neat or aqueous conditions (Figure 14c). Moreover, ceramic NPs can combine the chirality of the core or surface of the organic shell to induce enantioselectivity in catalysis. Wang et al.[178] reported the first photocatalytic asymmetric reduction of 3-methyl-2-oxobutanoic acid to yield 2-hydroxy-3-methylbutanoic acid with an enantiomeric excess of 60.0% using chiral BINAP-Rh(I) complexes and TiO_2 photocatalysts. Hu et al.[179] also designed Fe_3O_4-supported chiral Ru complexes that catalyze the heterogeneous asymmetric hydrogenation of aromatic ketones with very high enantiomeric excess (e.e.) values of up to 98.0%.[179] Kohtani et al.[180] modified the TiO_2 NPs with chiral mandelic acid and investigated the asymmetric induction in hydrogenation of aromatic ketones and found that the enantioselectivity was strongly affected by the TiO_2 crystalline samples. Fedorova et al.[181] investigated the catalytic effect of nanosized CuO, Al_2O_3, ZnO, NiO, and MgO with chiral inductors of L-Pro and L-tartaric acid in the Biginelli reaction. Nanosized metal oxides with chiral inductors increased the region- and stereoselectivity and the e.e. increased from 0% to 20%. The chiral molecules (menthol and Pro derivatives) noncovalent-functionalized TiO_2–SiO_2 were also used as catalysts for the Biginelli reaction with e.e. ranging from 0% to 22%.

4.4. Chiral Separation

Chiral recognition and separation processes are significant for drug development and biochemical studies and, in our opinion, chiral ceramic nanostructures have shown broad prospects in chiral recognition and separation. The enantioselective environment created by chiral ceramics is the key to recognition of the molecular chirality of enantiomers and the ability to achieve their separation.[182] Many chiral ligands that ceramics can be derivatized with including proteins,[183] cyclodextrin,[184] crown ethers,[185] oligo- and polysaccharides,[186] etc., have been developed for chiral recognition and separation. The combination of different chiral selectors, a variety of chiral and achiral ceramic nanostructures have been developed for efficient recognition and separation of enantiomers by various methods, for example, filtration, centrifugation, chromatography, high-performance liquid chromatography, etc.[16c,187]

Li and co-workers[188] coated bovine serum albumin on the surfaces of magnetic Fe_3O_4 NPs as a magnetic chiral composite selector for the separation of drug enantiomers (**Figure 15**a). The magnetic separation of racemic ibuprofen and ofloxacin provided the high e.e. value of 54% and 39%, respectively.[188] Ghosh et al.[189] found that the carboxymethyl-β-cyclodextrin-coated Fe_3O_4/SiO_2 NPs could selectively adsorb L-enantiomers of DL-tryptophan (DL-Trp), DL-phenylalanine (DL-Phe), and DL-tyrosine (DL-Tyr) from phosphate buffer solution.

Besides the stereoselectivity of chiral selectors, the physical interactions and assembly structure of chiral ceramics could also be applied in chiral recognition and selection. Wang's group was the first to find chiral recognition behavior in the self-assembly process of the wheel-shaped macroanions, $[Fe_{28}(\mu_3\text{-}O)_8(\text{L-tartaric acid})_{16}(HCOO)_{24}]^{20-}$ (L-Fe_{28}) and $[Fe_{28}(\mu_3\text{-}O)_8(\text{D-tartaric acid})_{16}(HCOO)_{24}]^{20-}$ (D-Fe_{28}) (Figure 15b).[190] The macroanions of L-Fe_{28} and D-Fe_{28} exhibited self-identification behavior and could individually be assembled to "blackberry" structures. The enantiomers of chiral co-anionic molecules (lactic acid or tartaric acid) can also selectively suppress the self-assembly process of macroanions in the presence of Ba^{2+} counterions. This is the result of the joint actions of compatibility and chiral microenvironment between chiral co-anions and the macroanions of L-Fe_{28} and D-Fe_{28} (Figure 15c). Based on long-range electrostatic interactions in the chiral microenvironment of D-lactic acid, L-Fe_{28} macroions dominantly self-assembled to "blackberry" structures, while most of D-Fe_{28} macroanions remained in the form of single clusters. Therefore, a racemic mixture of L-Fe_{28} and D-Fe_{28} with Ba^{2+} ions could be easily separated by filter membranes in the buffer of D-lactic acid, which is demonstrated in CD spectra (Figure 15d–f). Banerjee-Ghosh et al.[115] found that the introduction of spin polarization significantly affects enantiospecific recognition and can be used for effective separation of enantiomers. The design of different separation systems of chiral ceramics is guided by the electric and spin polarization properties of molecular enantiomers.

4.5. Biomedical and Biological Applications

Despite the well-known biocompatibility of ceramics, the research of chiral ceramic nanostructures related to bioapplications is, by and large, rare. The enantiomers of chiral drugs regularly exhibit different biological effects, which is mainly due to different enantiomer's preferential binding capabilities with target receptors. The enantiomers of chiral graphene or graphene quantum dots (GQDs) were reported to exhibit different toxicities to cells, including mammalian[191] and bacterial cells.[192] From atomistic simulations of the interaction between chiral GQDs and cellular membranes, our group found that, within the cellular membrane, the D-GQDs would aggregate more readily than L-GQDs.[191a] Ma et al.[193] prepared chiral POM-based porous films using the layer-by-layer (LBL) assembly method to deposit chiral POMs of L- and D-ZrP_2W_{15} inside the ordered cavernous film (**Figure 16**a). From *Escherichia coli* cell culture tests on different porous films, together with confocal laser scanning microscopy (CLSM) images, chiral POMs facilitate cell adhesion and proliferation (Figure 16b,c). Conversely, racemic porous films show high antibacterial properties. Based on knowledge that the cell adhesion starts from protein adsorption, the Ma group studied the interaction between model protein of BSA and the chiral or racemic surface to explain the cell adsorption. Quartz crystal microbalance (QCM) measurement demonstrated that the L-POM showed greater BSA adsorption capability than both the D-POM and racemic POM assembled resonators (Figure 16d).[193]
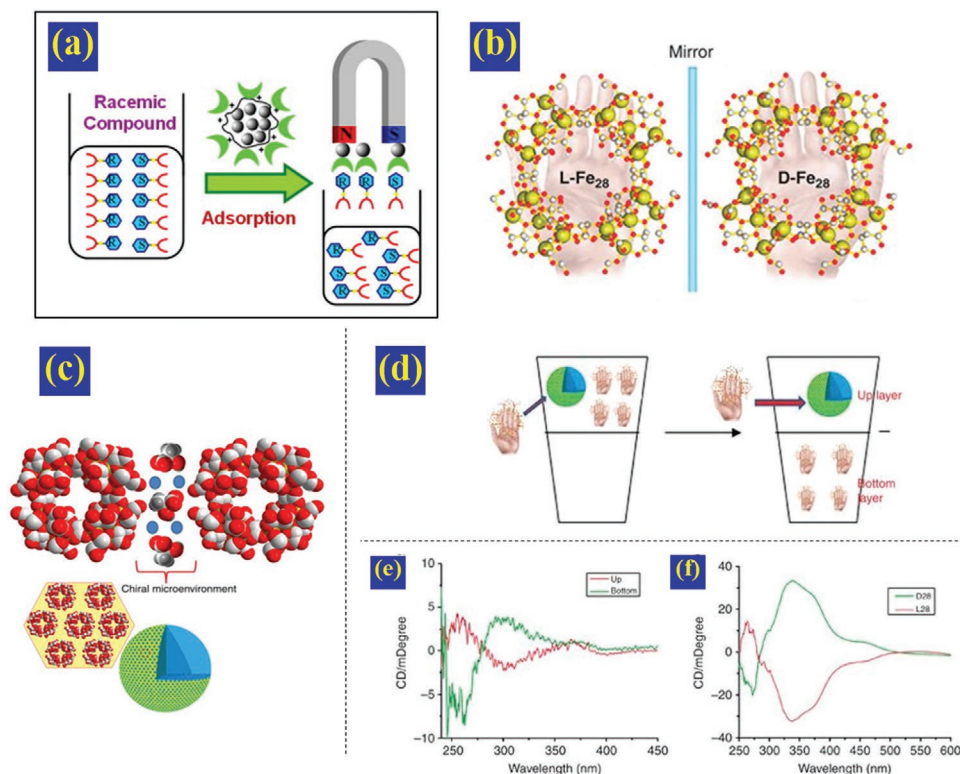
Figure 15. a) Chiral selector of bovine serum albumin-modified magnetic Fe_3O_4 NPs for enantiomeric adsorption. Reproduced with permission.[188] Copyright 2013, Elsevier B.V. b) Ball-and-stick representation of the macroanions of L-Fe_{28} and D-Fe_{28}. c) Self-assembly behavior of macroanions in a chiral microenvironment. Fe atom: yellow, O atom: red, Ba^{2+}: blue, C atom: light grey, H atom: dark grey. d) Chiral separation of Ba^{2+}-D-Fe_{28} and Ba^{2+}-L-Fe_{28} in the chiral microenvironment of D-lactic acid. e) CD spectra of Ba-L-Fe_{28} (red) and Ba-D-Fe_{28} (green) solutions after separation. f) CD spectra of pure Ba-L-Fe_{28} (red) and Ba-D-Fe_{28} (green) solutions. b–f) Reproduced with permission.[190] Copyright 2015, Springer Nature.

5. Summary and Future Prospects

The complexity and diversity of chiral ceramic nanostructures is quite remarkable and in this final section we focused on the preparation and potential applications of this rapidly evolving class of ceramic nanomaterials. While there has been notable progress in empirical studies with a wide range of potential applications, the field of chiral ceramic nanostructures remains full of challenges and opportunities. We expect chiral ceramic nanostructure research will experience rapid growth in the near future along the directions detailed below.

5.1. Expected Advances in Synthesis

5.1.1. Chiral Design of Ceramic Materials

Enantioselective synthesis of chiral ceramic nanostructures is the key to their applications in polarization-based optoelectronics, biomimetic catalysis, enantioselective separation, biomedical applications, and information technologies. The perfect control of handedness in chiral mesoporous ceramic nanostructures still is a challenge. The underlying microscopic mechanism for chiral reconstruction on the ceramic crystal induced by chiral ligands and their subsequent assembly into chiral superstructures must be studied in greater details and by applying novel scientific methods that include both experimental and computational techniques. The organization, distribution and dynamics of the chiral surface ligands on NP cores remains only partially understood for specific ceramic materials, such as Co_3O_4 or WO_{3-x}.[29,32] Knowledge gained from the CPL "templating" of NP's chiral assemblies and CPL-induced chiral plasmonic nanostructures may lead to the continuous expansion of fascinating developments in chiral ceramic nanostructures.[194] Different methods of modulation of chiroptical activity of chiral nanostructures, for example, optical vortex and magnetic field have great potential for the preparation of 3D isotropic chiral ceramic nanostructures. Strain-modulation with macroscopic gradients of biaxial strain fields is ideal for designing chiral ceramic nanocomposites by transferring chirality from macro to nanoscale. Employing ceramic particles as building blocks, the opto-thermophoretic assembly and optical tweezers should allow for rational manipulation of nanoscale colloidal particles so they can be assembled into chiral ceramic superstructures with new functions and use in optic devices.[195] For 2D chiral ceramic nanostructures, finding a facile method to realize chiral twisted van der Waals heterostructures with interlayer twists will be one of the major milestones in the future.

**ADVANCED
SCIENCE NEWS**

www.advancedsciencenews.com

**ADVANCED
MATERIALS**

www.advmat.de
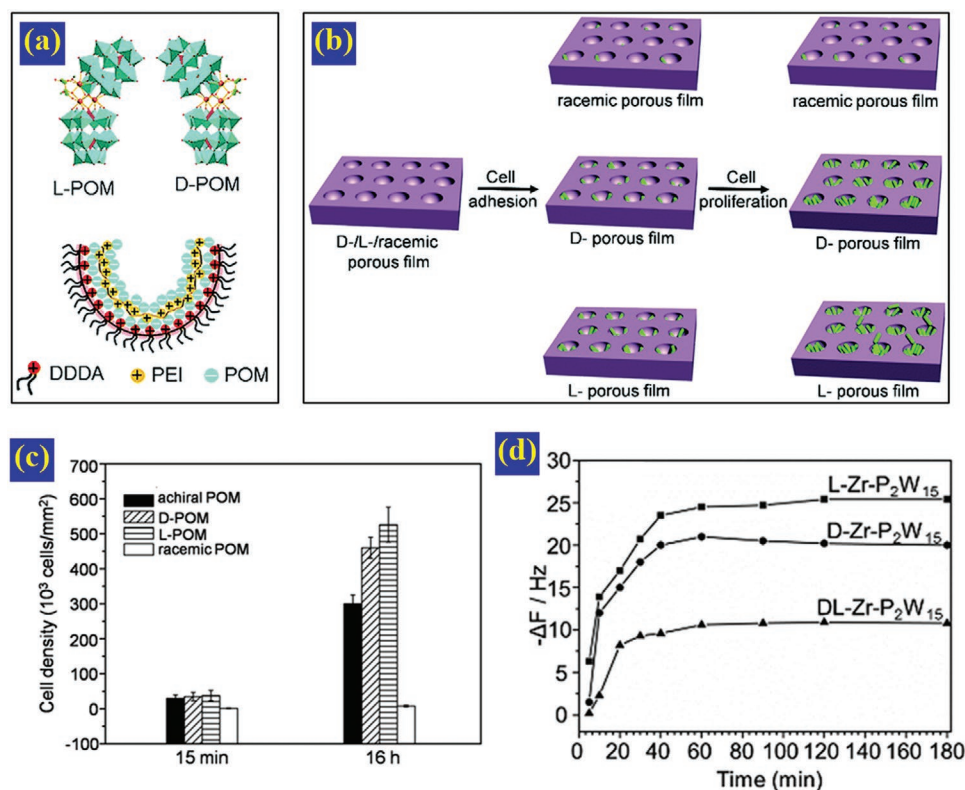
Figure 16. a) Schematics for LBL assembly of chiral POM. b) Cell adhesion and proliferation of different porous films. c) Counted numbers of *E. coli* cells adhered onto different porous films. d) Comparison of the adsorption behavior of different porous BSA films. a–d) Reproduced with permission.[193] Copyright 2019, Royal Society of Chemistry.

5.1.2. Composition and Structure

Based on the knowledge for chirality transfer and technological needs, it will be important to create a wide palette of individual ceramic NPs with a wide range of chiral ligands. This library will greatly enrich the chiral ceramic materials field and will enable applications of the new methods of materials discovery, based, for instance on machine learning. The interaction between the stereocenters of ligands and the NP core impact all their secondary physical, chemical, and biological properties. The relationship between CD, ROA, circularly polarized luminescence peaks, NP's geometry and crystal structures are worthy of further detailed examination. Incorporating chiral ceramic nanostructures with metal or semiconductor NPs through surface loading and internal embedding will generate more interesting optical activity. Excluding individual NPs, structural adjustment will continue to be a primary focus in the development chiral ceramic nanostructures.

No single mechanism can explain the chirality transfer in nanostructures. Therefore, in-depth study with integrated chiral assembly mechanisms is paramount for us to understand the specific chiral assembly processes of chiral ceramic nanostructures, especially for supramolecular chiral materials from achiral molecules to surfactants. The design of chiral surfaces and channels in chiral POMs, metal-organic coordination polymers, and zeolites will continue to be the main topic for enantioselective catalysis. In this respect, we can point out the importance of collective interactions for the chiral assemblies

and surfaces. The current theories of NPs interactions are insufficient to address them,[196] and their development can be facilitated by the studies of chiral nanoassemblies. One example can be the application of classical methods of statistical mechanics to chiral nanostructures based on lanthanide phosphate by Hananel et al.[197] that revealed strong amplification of chirality. These findings are in direct agreement with the previous observations of nearly perfect enantioselective assemblies of chiral nanoparticles into either left- or right-handed helices.[196]

The routes to chiral ceramic nanostructures, including template-guided synthesis and the vapor deposition process, will provide a basis for diverse structural syntheses, which will lead to more and more unique chiral structural ceramics, for example, core–shell structures, hollow structures, and heterogeneous structures. The growth of chiral ceramic spirals and helices could give rise to defects and exposure of active crystal faces, which will boost catalytic activity. The construction of hierarchical, or heterogeneous, structures is imperative for successful regulation of the optical activity of chiral ceramics across the wide range of electromagnetic spectrum from X-ray to microwave frequencies.

5.2. Computational Methods Chiral Nanostructures

The development of chirality-related computational methods will enable the exploration of the mechanisms by which optical activity is generated in chiral ceramic nanostructures and also

help to explain experimental data from any type of chiral nanomaterials. Comparing with semiconductor and metallic nanostructures, ceramics presents results in chiral structures from lighter elements, which is always beneficial for high-level computations. Comparison of experimental and theoretically predicted optical activity was a significant approach for the study of conformational changes. Geometry optimization and ab initio molecular dynamics with integration of density functional theory, can be expanded much further because they are needed for validation of structural transformations in NPs and their superstructures. These methods not only can visualize chiral distortions but can also explain the fine details of the interactions between chiral ligands and ceramic surfaces.

Computational methods addressing the atomistic structure of nanostructures and specifically chiral ceramics should be thoroughly validated by comparing the computational predictions and experimental data. Although much progress was made in this area using CD and circularly polarized luminescence data, the protocols for such validations are still being developed. In our opinion, wider use of ROA, vibrational circular dichroism (VCD), and terahertz circular dichroism (TCD)[198] could provide needed molecular, nano, and mesoscale level information about dynamics and equilibrium states of chiral nanostructures that would be of great value for rapid validation of computational methods. In perspective, integration of all of these methods can provide path to establish absolute configuration of chiral nanostructures based exclusively on the combination of spectroscopic and simulation data, which was so far a daunting task. For example, time-dependent density functional theory (TDDFT) is widely used for the interpretation of CD spectra toward identification of absolute configuration. However, TDDFT is not universally accurate, with major limitations including charge transfer and Rydberg excitations, as well as double and higher excitations.[191a] Recently, Tang and co-workers[199] used the nondegenerate coupled oscillator (NDCO) model to explain the optical activity of chiral CdSe quantum rods in both the UV and the visible regions by considering the cysteine, Cd−S bond, and QRs as three different chromophores. However, for more complex chiral structures with chromophores very close to each other, the NDCO model is not applicable. Therefore, breakthrough improvements in TDDFT and NDCO theoretical models are expected. Emerging hybrid quantum mechanics and molecular mechanics simulations are worthy of attention for the investigation of the condensed phases. Looking ahead, geometry optimizations and ab initio molecular dynamics (AIMD) simulations might not be able to solve all the problem that arise

from the interaction between radiation and nanostructures or interactions between multiple NPs due to high computational costs and temporal limits of structural evolution that these methods can model. Thus, we project expansion of the use of coarse grained MD methods, when effective potentials are used for specific chiral groups.[200] Electrodynamic simulations based on finite element discretization are widely used for chiral plasmonic structures from metals and some semiconductors, but have been not yet applied to chiral ceramics. Given the high accuracy of predictions for CD spectra of mesoscale structures from metals and semiconductors, one should expect the same for chiral ceramics. This effort will also benefit a large variety of their applications, because it will allow a priori computational design of chiroptical activity.

5.3. Emerging Applications

5.3.1. Modulation of Chiroptical Activity

The enhancement of chiroptical activity toward high *g*-factors is expected to be one of the important research directions in chiral ceramic nanostructures. Considerable attempts were made in achieving high values of *g*-factors for chiral nanoceramics (**Table 1**).[22b,38,201] Methods to mitigate absorption from ceramic nanostructures while maximizing polarization rotation should be elaborated. In this respect chiral nanoceramics is likely to have an advantage over the semiconductor and metal nanostructures because high values of *g*-factors can be obtained via enhancement of local magnetic rather than electrical field in chiral superstructures.[30,202] Furthermore, combining and controlling the dielectric and plasmonic contributions into chiroptical effects is also possible. The chiral MoO_{3-x} NPs mentioned above revealed their adjustable optical activity due to strong delocalization of electrons that is similar to chiroplasmonic nanostructures from noble metals.[39] Some ceramic nanomaterials, such as conductive transition metal oxides and metal nitrides, are already known to exhibit surface plasmon resonance,[203] and therefore, one might expect that ceramic nanostructures with strong chiroplasmonic effects will be given significant attention in the next decade. Chiral ceramic nanostructures with strong circularly polarized luminescence are also expected to be realized. The major driver for their research will be the next-generation of display and storage devices. Both directions can benefit from theoretical studies of local superchiral fields.[204] Finite-difference-time-domain (FDTD)

Table 1. Typical values of *g*-factors found for chiral nanoceramics.

Chiral nanoceramics	Ligands	Wavelength [nm]	*g*-Factor	References
Chiral WO_{3-x} NPs	L- and D-Asp	≈1100	$<3.5 \times 10^{-4}$	[38]
	L- and D-Pro	560	1.83×10^{-3}	[38]
Chiral MoO_2 NPs	L- and D-Cysteine	580	$≈7 \times 10^{-3}$	[39]
Chiral MoO_{3-x} NPs	L- and D-Cysteine	580	$≈1 \times 10^{-4}$	[39]
Chiral Co_3O_4 NPs	L-Cysteine	550	0.02	[22b]
Chiral TiO_2 NPs	L-Ascorbic acid	500	3.0×10^{-4}	[201b]
	L-Noradrenaline	500	0.80×10^{-4}	[201b]

simulation provides a powerful toolbox to understand the physical origins of the CD spectra for individual NPs and NP assemblies. By comparative analysis of experimental and simulated CD and *g*-factor spectra, the effects of symmetry-breaking and geometrical parameters on chiroptical activities of chiral nanoceramics could be understood and then guide the synthesis of chiral ceramic nanostructures. From the theory of CD signals related to chiral nanoceramics including the nanocrystals and chiral ligands, the optical chirality of chiral ceramic nanostructures also can be enhanced and tailored by plasmon enhancement, dipole interactions, and dielectric effects.[205] On the basis of the energetically and thermodynamically stable conformation and configuration of chiral ceramic nanostructures predicted by MD simulations, more and more chiral ceramic materials can be developed rationally.

Field modulation of chiroptical activity is expected to be a rapidly growing part of research on all chiral nanostructures being fueled by rapid expansion of polarization-based optoelectronics and metamaterials. Control of chiroptical activity, for example, by magnetic field,[32] can bring about multiple discoveries in respect to chiromagnetic effects and nonlinear optics enables by chiral ceramic nanostructures. Realization of polarization modulation by electric fields will be beneficial for the numerous applications of chiral ceramics in optics and conducive with the characteristics of ceramic materials in general. In this respect, Sargent and co-workers[206] reported the spin polarization in reduced-dimensional perovskites could be controlled by magnetic field which will lay the foundation of chiral perovskites for spintronic materials. Moreover, chiral nematic liquid crystalline phases of ceramic nanomaterials may be of interest for photochromic, display, and storage devices. Zhao and Alù[207] found that the strong polarization conversion and quarter-wave plate functionality can be achieved using chiral ITO-based planar metasurface patterned with silver NRs orthogonal array. The design principles will show great potential in control of the transmitted phase and can be extended to cover the visible, near-infrared, and even THz range. The useful fact that should not to be ignored is that terahertz radiation can pass through ceramics.[198,208] The chiral ceramic metamaterials in the THz portion of the spectrum including application of TCD to study biomaterials are just starting to bloom.[198]

5.3.2. Site-Specific Catalysis

Similarly to findings that chiral $Cu_{2-x}S$ nanocrystals show site selectivity in scission of protein macromolecules under circularly polarized light irradiation,[209] one might expect that chiral ceramic nanostructures with redox-active plasmonic and excitonic states could also be used for the similar purposes and in fact, be more specific. While current understanding of the origin of site-selectivity is related to supramolecular interactions of chiral NPs and biopolymers—DNA or proteins—other mechanisms may also be possible.[210] Furthermore, the identification of cleavage sites in protein cutting and prediction of the produced peptides using versatile chemistry of chiral ceramics including, for instance copper and cobalt oxides can be the focus of future studies. In principle, this may open the path to DNA- and protein-modification technologies based on chiral ceramics. Based on the current knowledge of NP assemblies and specificity of supramolecular interactions between them and biomolecules, it is conceptually possible to create gene-editing toolbox based on inorganic materials utilizing circularly polarized photons. As the near-term target-site-specific catalytic hydrolysis of lignin, polysaccharide, starch, and cellulose may also be appealing as a chemical path to chiral high-value products from the biomass.

Herein, the relationship between synthetic methods and chiral structure is studied using multiple examples of synthetic methods for preparing chiral ceramic nanostructures. Next, we discuss the recent progress of chiral ceramic nanostructures, focusing on ceramic oxides, polyoxometalates (POMs), and zeolites. The chirality transfers from molecular scale to nanoscale and higher to microscale are discussed as applied for ceramic nanostructures. Taking advantage of these nearly universal approaches, a diverse spectrum of ceramic nanostructures with unique properties can be engineered. The review ends with our perspective on the future developments of chiral ceramic nanostructures in terms of their preparation and applications encompassing both traditional (e.g., enantioselective catalysis) and emerging (e.g., quantum optics) technologies.

5.3.3. Quantum Information Technologies

In the field of quantum information science, theoretical studies on chiral topological superconductors promote novel quasi-2D topological ceramic superconducting systems to detect and braid Majorana fermions. Research on the chiral stacking of 2D ceramic nanomaterials in lateral and vertical directions could open new horizons in superconductivity and related mechanisms. Chiral twisted van der Waals ceramic heterostructure will expose more and more attractive properties of condensed matter physics.[20a] Atomic coupled doping in 2D ceramic nanomaterials can derive novel spintronic materials and will provide chances to regulate the phase of the Majorana state with magnetic fields. Chiral quantum optic components represent the future of quantum networks for processing quantum information in quantum computers.[211] Development of new transmission electron microscopy tools that enable probing of nanometer and sub-nanometer-scale chirality in solids[212] will help designing chiral ceramics for quantum technologies.

In light of the unique physical and chemical properties of ceramic materials, the field of chiral ceramic nanostructures is full of challenges and opportunities. The development of chiral ceramic materials will significantly expand the field of chiral research, and, ultimately help us to understand the asymmetry laws of nature and life.

Acknowledgements

Conflict of Interest

The authors declare no conflict of interest.

Keywords

biomimetic helices, chiroplasmonics, metal oxides, mirror asymmetry, nanoassemblies

[1] a) R. S. Cahn, C. Ingold, V. Prelog, *Angew. Chem., Int. Ed. Engl.* **1966**, *5*, 385; b) Y. Wang, J. Xu, Y. Wang, H. Chen, *Chem. Soc. Rev.* **2013**, *42*, 2930.

[2] a) H. Flack, *Acta Crystallogr., Sect. A: Found. Crystallogr.* **2009**, *65*, 371; b) L. Pasteur, *Ann. Chim. Phys.* **1848**, *24*, 442.

[3] a) V. V. Borovkov, G. A. Hembury, Y. Inoue, *Acc. Chem. Res.* **2004**, *37*, 449; b) V. Farina, J. T. Reeves, C. H. Senanayake, J. J. Song, *Chem. Rev.* **2006**, *106*, 2734; c) W. H. Brooks, W. C. Guida, K. G. Daniel, *Curr. Top. Med. Chem.* **2011**, *11*, 760; d) J. R. Brandt, F. Salerno, M. J. Fuchter, *Nat. Rev. Chem.* **2017**, *1*, 0045; e) D. R. Boyd, M. A. McKervey, *Q. Rev., Chem. Soc.* **1968**, *22*, 95.

[4] a) M. Inaki, J. Liu, K. Matsuno, *Philos. Trans. R. Soc., B* **2016**, *371*, 20150403; b) D. G. Blackmond, *Cold Spring Harbor Perspect. Biol.* **2010**, *2*, a002147.

[5] a) R. Naaman, Y. Paltiel, D. H. Waldeck, *Nat. Rev. Chem.* **2019**, *3*, 250; b) M. Senami, K. Ito, *Phys. Rev. A* **2019**, *99*, 012509; c) A. Dorta-Urra, P. Bargueño, *Symmetry* **2019**, *11*, 661; d) P. L. Guennec, *J. Math. Phys.* **2000**, *41*, 5954; e) M. Goldhaber, L. Grodzins, A. W. Sunyar, *Phys. Rev.* **1958**, *109*, 1015.

[6] a) R. Kafri, O. Markovitch, D. Lancet, *Biol. Direct* **2010**, *5*, 38; b) L. A. Nguyen, H. He, C. Pham-Huy, *Int. J. Biomed. Sci.* **2006**, *2*, 85; c) A. Berthod, *Anal. Chem.* **2006**, *78*, 2093.

[7] W. Ma, L. Xu, A. F. de Moura, X. Wu, H. Kuang, C. Xu, N. A. Kotov, *Chem. Rev.* **2017**, *117*, 8041.

[8] T. G. Schaaff, R. L. Whetten, *J. Phys. Chem. B* **2000**, *104*, 2630.

[9] M. P. Moloney, Y. K. Gun'ko, J. M. Kelly, *Chem. Commun.* **2007**, 3900.

[10] Y. Zhou, M. Yang, K. Sun, Z. Tang, N. A. Kotov, *J. Am. Chem. Soc.* **2010**, *132*, 6006.

[11] A. S. Baimuratov, I. D. Rukhlenko, R. E. Noskov, P. Ginzburg, Y. K. Gun'ko, A. V. Baranov, A. V. Fedorov, *Sci. Rep.* **2015**, *5*, 14712.

[12] a) W. Chen, A. Bian, A. Agarwal, L. Liu, H. Shen, L. Wang, C. Xu, N. A. Kotov, *Nano Lett.* **2009**, *9*, 2153; b) B. M. Maoz, R. van der Weegen, Z. Fan, A. O. Govorov, G. Ellestad, N. Berova, E. W. Meijer, G. Markovich, *J. Am. Chem. Soc.* **2012**, *134*, 17807; c) B. Auguié, J. L. Alonso-Gómez, A. Guerrero-Martínez, L. M. Liz-Marzán, *J. Phys. Chem. Lett.* **2011**, *2*, 846.

[13] a) K. Ngamdee, W. Ngeontae, *Sens. Actuators, B.* **2018**, *274*, 402; b) Y. Wang, X. Zhou, C. Xu, Y. Jin, B. Li, *Sci. Rep.* **2018**, *8*, 5296; c) Y. Xia, Y. Zhou, Z. Tang, *Nanoscale* **2011**, *3*, 1374.

[14] a) I. Söllner, S. Mahmoodian, S. L. Hansen, L. Midolo, A. Javadi, G. Kiršanskė, T. Pregnolato, H. El-Ella, E. H. Lee, J. D. Song, S. Stobbe, P. Lodahl, *Nat. Nanotechnol.* **2015**, *10*, 775; b) W. Ma, H. Kuang, L. Wang, L. Xu, W.-S. Chang, H. Zhang, M. Sun, Y. Zhu, Y. Zhao, L. Liu, C. Xu, S. Link, N. A. Kotov, *Sci. Rep.* **2013**, *3*, 1934; c) M. Hentschel, M. Schäferling, X. Duan, H. Giessen, N. Liu, *Sci. Adv.* **2017**, *3*, e1602735.

[15] a) L. Kang, S. Lan, Y. Cui, S. P. Rodrigues, Y. Liu, D. H. Werner, W. Cai, *Adv. Mater.* **2015**, *27*, 4377; b) F. Zinna, U. Giovanella, L. D. Bari, *Adv. Mater.* **2015**, *27*, 1791; c) M. M. Glazov, S. D. Ganichev, *Phys. Rep.* **2014**, *535*, 101; d) P. M. Perez-Piskunow, G. Usaj, C. A. Balseiro, L. E. F. F. Torres, *Phys. Rev. B* **2014**, *89*, 121401.

[16] a) N. Shukla, M. A. Bartel, A. J. Gellman, *J. Am. Chem. Soc.* **2010**, *132*, 8575; b) C. F. McFadden, P. S. Cremer, A. J. Gellman, *Langmuir* **1996**, *12*, 2483; c) A. Gogoi, N. Mazumder, S. Konwer, H. Ranawat, N.-T. Chen, G.-Y. Zhuo, *Molecules* **2019**, *24*, 1007.

[17] a) K. Sawai, R. Tatumi, T. Nakahodo, H. Fujihara, *Angew. Chem., Int. Ed.* **2008**, *47*, 6917; b) C. Hao, R. Gao, Y. Li, L. Xu, M. Sun, C. Xu, H. Kuang, *Angew. Chem.* **2019**, *131*, 7449; c) S. Zhao, F. Caruso, L. Dähne, G. Decher, B. G. De Geest, J. Fan, N. Feliu, Y. Gogotsi, P. T. Hammond, M. C. Hersam, A. Khademhosseini, N. Kotov, S. Leporatti, Y. Li, F. Lisdat, L. M. Liz-Marzán, S. Moya, P. Mulvaney, A. L. Rogach, S. Roy, D. G. Shchukin, A. G. Skirtach, M. M. Stevens, G. B. Sukhorukov, P. S. Weiss, Z. Yue, D. Zhu, W. J. Parak, *ACS Nano* **2019**, *13*, 6151.

[18] a) K. Unfried, C. Albrecht, L.-O. Klotz, A. Von Mikecz, S. Grether-Beck, R. P. F. Schins, *Nanotoxicology* **2007**, *1*, 52; b) N. Suzuki, Y. Wang, P. Elvati, Z.-B. Qu, K. Kim, S. Jiang, E. Baumeister, J. Lee, B. Yeom, J. H. Bahng, J. Lee, A. Violi, N. A. Kotov, *ACS Nano* **2016**, *10*, 1744.

[19] a) C.-Y. Sun, C. Qin, C.-G. Wang, Z.-M. Su, S. Wang, X.-L. Wang, G.-S. Yang, K.-Z. Shao, Y.-Q. Lan, E.-B. Wang, *Adv. Mater.* **2011**, *23*, 5629; b) Z. Guo, Y. Du, X. Liu, S.-C. Ng, Y. Chen, Y. Yang, *Nanotechnology* **2010**, *21*, 165103; c) A. Motealleh, P. Dorri, N. S. Kehr, *J. Mater. Chem. B* **2019**, *7*, 2362; d) H. Li, H. Li, C. Wei, J. Ke, J. Li, L. Xu, H. Liu, YangYang, S. Li , M. Yang, *Eur. J. Pharm. Sci.* **2018**, *117*, 321.

[20] a) M. Sun, L. Xu, A. Qu, P. Zhao, T. Hao, W. Ma, C. Hao, X. Wen, F. M. Colombari, A. F. de Moura, N. A. Kotov, C. Xu, H. Kuang, *Nat. Chem.* **2018**, *10*, 821; b) S. Li, J. Liu, N. S. Ramesar, H. Heinz, L. Xu, C. Xu, N. A. Kotov, *Nat. Commun.* **2019**, *10*, 4826; c) X. Feng, H. S. Jena, K. Leus, G. Wang, J. Ouwehand, P. Van Der Voort, *J. Catal.* **2018**, *365*, 36; d) C. Li, H. Zhang, D. Jiang, Q. Yang, *Chem. Commun.* **2007**, 547.

[21] a) W. Jiang, X. Yi, M. D. McKee, *Mater. Horiz.* **2019**, *6*, 1974; b) B. Sung, A. de la Cotte, E. Grelet, *Nat. Commun.* **2018**, *9*, 1405; c) Z. Guo, J. Wang, F. Qin, W. Shen, *J. Colloid Interface Sci.* **2019**, *543*, 130; d) S. Elsharkawy, A. Mata, *Adv. Healthcare Mater.* **2018**, *7*, 1800178;

[22] a) C. O. Avci, E. Rosenberg, L. Caretta, F. Büttner, M. Mann, C. Marcus, D. Bono, C. A. Ross, G. S. D. Beach, *Nat. Nanotechnol.* **2019**, *14*, 561; b) J. Yeom, U. S. Santos, M. Chekini, M. Cha, A. F. de Moura, N. A. Kotov, *Science* **2018**, *359*, 309; c) T. Weber, J. Waizner, G. S. Tucker, R. Georgii, M. Kugler, A. Bauer, C. Pfleiderer, M. Garst, P. Böni, *Phys. Rev. B* **2018**, *97*, 224403; d) D.-W. Wang, C. Song, W. Feng, H. Cai, D. Xu, H. Deng, H. Li, D. Zheng, X. Zhu, H. Wang, S.-Y. Zhu, M. O. Scully, *Nat. Phys.* **2019**, *15*, 382; e) B. Liu, P. Zhang, H. Gao, F. Li, *Phys. Rev. Lett.* **2018**, *121*, 015303.

[23] a) M. J. Urban, C. Shen, X.-T. Kong, C. Zhu, A. O. Govorov, Q. Wang, M. Hentschel, N. Liu, *Annu. Rev. Phys. Chem.* **2019**, *70*, 275; b) J.-W. Chen, T. Ishii, S. Pu, N. Yamamoto, *Phys. Rev. D* **2016**, *93*, 125023; c) A. Mukherjee, S. Schramm, J. Steinheimer, V. Dexheimer, *Astron. Astrophys.* **2017**, *608*, A110.

**ADVANCED
SCIENCE NEWS**

www.advancedsciencenews.com

**ADVANCED
MATERIALS**

www.advmat.de

[24] a) C. C. Kolb, in *Encyclopedia of Geoarchaeology* (Ed: A. S. Gilbert), Springer, Dordrecht, Netherlands **2017**, p. 118; b) Z.-B. Qu, W.-J. Feng, Y. Wang, F. Romanenko, N. A. Kotov, *Angew. Chem., Int. Ed.* **2020**, *59*, 8542; c) N. A. Kotov, *Europhys. Lett.* **2017**, *119*, 66008; d) J. J. De Yoreo, P. U. P. A. Gilbert, N. A. J. M. Sommerdijk, R. L. Penn, S. Whitelam, D. Joester, H. Zhang, J. D. Rimer, A. Navrotsky, J. F. Banfield, A. F. Wallace, F. M. Michel, F. C. Meldrum, H. Cölfen, P. M. Dove, *Science* **2015**, *349*, aaa6760; e) M. F. Hochella, D. W. Mogk, J. Ranville, I. C. Allen, G. W. Luther, L. C. Marr, B. P. McGrail, M. Murayama, N. P. Qafoku, K. M. Rosso, N. Sahai, P. A. Schroeder, P. Vikesland, P. Westerhoff, Y. Yang, *Science* **2019**, *363*, eaau8299.

[25] I. Denry, J. A. Holloway, *Materials* **2010**, *3*, 351.

[26] a) M. Rosso, *J. Mater. Process. Technol.* **2006**, *175*, 364; b) R. J. Brook, in *Concise Encyclopedia of Advanced Ceramic Materials* (Ed: R. J. Brook), Pergamon Press, Oxford, UK **1991**, p. 1.

[27] C. B. Carter, M. G. Norton, *Ceramic Materials: Science and Engineering*, Springer, New York **2013**, p. 3.

[28] G. Mera, M. Gallei, S. Bernard, E. Ionescu, *Nanomaterials* **2015**, *5*, 468.

[29] J. Gal, *Chirality* **2011**, *23*, 1.

[30] K. Soai, S. Osanai, K. Kadowaki, S. Yonekubo, T. Shibata, I. Sato, *J. Am. Chem. Soc.* **1999**, *121*, 11235.

[31] a) S. K. Brand, J. E. Schmidt, M. W. Deem, F. Daeyaert, Y. Ma, O. Terasaki, M. Orazov, M. E. Davis, *Proc. Natl. Acad. Sci. USA* **2017**, *114*, 5101; b) C. Dryzun, Y. Mastai, A. Shvalb, D. Avnir, *J. Mater. Chem.* **2009**, *19*, 2062.

[32] a) Y. Han, Y. Li, J. Yu, R. Xu, *Angew. Chem., Int. Ed.* **2011**, *50*, 3003; b) L. Tang, L. Shi, C. Bonneau, J. Sun, H. Yue, A. Ojuva, B.-L. Lee, M. Kritikos, R. G. Bell, Z. Bacsik, J. Mink, X. Zou, *Nat. Mater.* **2008**, *7*, 381.

[33] a) A. Ben-Moshe, A. O. Govorov, G. Markovich, *Angew. Chem., Int. Ed.* **2013**, *52*, 1275; b) F. P. Milton, J. Govan, M. V. Mukhina, Y. K. Gun'ko, *Nanoscale Horiz.* **2016**, *1*, 14.

[34] R. M. Hazen, D. A. Sverjensky, *Cold Spring Harbor Perspect. Biol.* **2010**, *2*, a002162.

[35] a) G. Danger, R. Plasson, R. Pascal, *Chem. Soc. Rev.* **2012**, *41*, 5416; b) T. Georgelin, M. Jaber, H. Bazzi, J.-F. Lambert, *Origins Life Evol. Biospheres* **2013**, *43*, 429; c) A. Rimola, M. Sodupe, P. Ugliengo, *Life* **2019**, *9*, 10.

[36] J. Kumar, K. G. Thomas, L. M. Liz-Marzán, *Chem. Commun.* **2016**, *52*, 12555.

[37] O. Cleary, F. Purcell-Milton, A. Vandekerckhove, Y. K. Gun'ko, *Adv. Opt. Mater.* **2017**, *5*, 1601000.

[38] S. Jiang, M. Chekini, Z.-B. Qu, Y. Wang, A. Yeltik, Y. Liu, A. Kotlyar, T. Zhang, B. Li, H. V. Demir, N. A. Kotov, *J. Am. Chem. Soc.* **2017**, *139*, 13701.

[39] Y. Li, J. Cheng, J. Li, X. Zhu, T. He, R. Chen, Z. Tang, *Angew. Chem.* **2018**, *130*, 10393.

[40] a) Z. Zhou, F. Zhang, J. Wang, X. Zhang, W. Xu, R. Wu, L. Liao, X. Wang, J. Wei, *Mater. Sci. Eng., C* **2019**, *103*, 109818; b) A. Sandmann, A. Kompch, V. Mackert, C. H. Liebscher, M. Winterer, *Langmuir* **2015**, *31*, 5701; c) E. Chwojnowska, M. Wolska-Pietkiewicz, J. Grzonka, J. Lewiński, *Nanoscale* **2017**, *9*, 14782.

[41] A. Ben-Moshe, B. M. Maoz, A. O. Govorov, G. Markovich, *Chem. Soc. Rev.* **2013**, *42*, 7028.

[42] S. Kim, J.-M. Kim, J.-E. Park, J.-M. Nam, *Adv. Mater.* **2018**, *30*, 1704528.

[43] a) W. Ma, C. Hao, M. Sun, L. Xu, C. Xu, H. Kuang, *Mater. Horiz.* **2018**, *5*, 141; b) E. Yashima, N. Ousaka, D. Taura, K. Shimomura, T. Ikai, K. Maeda, *Chem. Rev.* **2016**, *116*, 13752; c) J. H. Jung, M. Park, S. Shinkai, *Chem. Soc. Rev.* **2010**, *39*, 4286.

[44] H. Qiu, S. Che, *Chem. Soc. Rev.* **2011**, *40*, 1259.

[45] C. Zhang, S. Wang, H. Huo, Z. Huang, Y. Li, B. Li, Y. Yang, *Chem. - Asian J.* **2013**, *8*, 709.

[46] S. Yang, L. Zhao, C. Yu, X. Zhou, J. Tang, P. Yuan, D. Chen, D. Zhao, *J. Am. Chem. Soc.* **2006**, *128*, 10460.

[47] H. Huo, S. Wang, S. Lin, Y. Li, B. Li, Y. Yang, *J. Mater. Chem. A* **2014**, *2*, 333.

[48] Q. Wang, S. Lin, J. Qin, Y. Li, B. Li, Y. Yang, *Chirality* **2016**, *28*, 44.

[49] A. Sola-Rabada, M.-K. Liang, M. J. Roe, C. C. Perry, *J. Mater. Chem. B* **2015**, *3*, 3777.

[50] a) B. Liu, Y. Cao, Z. Huang, Y. Duan, S. Che, *Adv. Mater.* **2015**, *27*, 479; b) M. Numata, K. Sugiyasu, T. Hasegawa, S. Shinkai, *Angew. Chem., Int. Ed.* **2004**, *43*, 3279.

[51] a) Z. Wu, Y. Yan, J. Huang, *Langmuir* **2014**, *30*, 14375; b) Y. Qiao, Y. Lin, Y. Wang, Z. Yang, J. Liu, J. Zhou, Y. Yan, J. Huang, *Nano Lett.* **2009**, *9*, 4500; c) Y. Qiao, Y. Wang, Z. Yang, Y. Lin, J. Huang, *Chem. Mater.* **2011**, *23*, 1182.

[52] a) Y. Yang, M. Suzuki, S. Owa, H. Shirai, K. Hanabusa, *J. Mater. Chem.* **2006**, *16*, 1644; b) Y. Yang, M. Suzuki, H. Shirai, A. Kurose, K. Hanabusa, *Chem. Commun.* **2005**, 2032; c) T. Yokoi, Y. Yamataka, Y. Ara, S. Sato, Y. Kubota, T. Tatsumi, *Microporous Mesoporous Mater.* **2007**, *103*, 20; d) S. Che, Z. Liu, T. Ohsuna, K. Sakamoto, O. Terasaki, T. Tatsumi, *Nature* **2004**, *429*, 281; e) H. Jin, Z. Liu, T. Ohsuna, O. Terasaki, Y. Inoue, K. Sakamoto, T. Nakanishi, K. Ariga, S. Che, *Adv. Mater.* **2006**, *18*, 593; f) K. Sugiyasu, S.-i. Tamaru, M. Takeuchi, D. Berthier, I. Huc, R. Oda, S. Shinkai, *Chem. Commun.* **2002**, 1212.

[53] a) A. M. Seddon, H. M. Patel, S. L. Burkett, S. Mann, *Angew. Chem., Int. Ed.* **2002**, *41*, 2988; b) J. H. Jung, Y. Ono, S. Shinkai, *Angew. Chem., Int. Ed.* **2000**, *39*, 1862; c) Y. Yang, M. Suzuki, S. Owa, H. Shirai, K. Hanabusa, *J. Am. Chem. Soc.* **2007**, *129*, 581; d) J. H. Jung, S.-H. Lee, J. S. Yoo, K. Yoshida, T. Shimizu, S. Shinkai, *Chem. - Eur. J.* **2003**, *9*, 5307.

[54] a) B. Wang, C. Chi, W. Shan, Y. Zhang, N. Ren, W. Yang, Y. Tang, *Angew. Chem., Int. Ed.* **2006**, *45*, 2088; b) Y. Han, L. Zhao, J. Y. Ying, *Adv. Mater.* **2007**, *19*, 2454.

[55] H. Qiu, S. Che, *J. Phys. Chem. B* **2008**, *112*, 10466.

[56] H. Ogihara, M. Sadakane, Y. Nodasaka, W. Ueda, *Chem. Mater.* **2006**, *18*, 4981.

[57] Y. Qin, Y. Kim, L. Zhang, S.-M. Lee, R. B. Yang, A. Pan, K. Mathwig, M. Alexe, U. Gösele, M. Knez, *Small* **2010**, *6*, 910.

[58] K. E. Shopsowitz, H. Qi, W. Y. Hamad, M. J. MacLachlan, *Nature* **2010**, *468*, 422.

[59] G. Chu, J. Feng, Y. Wang, X. Zhang, Y. Xu, H. Zhang, *Dalton Trans.* **2014**, *43*, 15321.

[60] a) P. X. Gao, Y. Ding, W. Mai, W. L. Hughes, C. Lao, Z. L. Wang, *Science* **2005**, *309*, 1700; b) Z. L. Wang, *J. Mater. Chem.* **2005**, *15*, 1021.

[61] Z. Y. Zhang, X. L. Wu, L. L. Xu, J. C. Shen, G. G. Siu, P. K. Chu, *J. Chem. Phys.* **2008**, *129*, 164702.

[62] R. Yang, Z. L. Wang, *J. Am. Chem. Soc.* **2006**, *128*, 1466.

[63] X. Wang, G. Xi, S. Xiong, Y. Liu, B. Xi, W. Yu, Y. Qian, *Cryst. Growth Des.* **2007**, *7*, 930.

[64] G. Shen, D. Chen, *J. Am. Chem. Soc.* **2006**, *128*, 11762.

[65] C. Wu, H. Zhu, J. Dai, W. Yan, J. Yang, Y. Tian, S. Wei, Y. Xie, *Adv. Funct. Mater.* **2010**, *20*, 3666.

[66] C.-Y. Xu, J. Wu, L.-X. Lv, J.-X. Cui, Z.-Q. Wang, Y.-D. Huang, L. Zhen, *CrystEngComm* **2011**, *13*, 2674.

[67] C.-Y. Xu, Y.-Z. Liu, L. Zhen, Z. L. Wang, *J. Phys. Chem. C* **2008**, *112*, 7547.

[68] S. Y. Bae, J. Lee, H. Jung, J. Park, J.-P. Ahn, *J. Am. Chem. Soc.* **2005**, *127*, 10802.

[69] H. S. Kim, S. O. Hwang, Y. Myung, J. Park, S. Y. Bae, J. P. Ahn, *Nano Lett.* **2008**, *8*, 551.

[70] a) A. Barranco, A. Borras, A. R. Gonzalez-Elipe, A. Palmero, *Prog. Mater. Sci.* **2016**, *76*, 59; b) B. Ai, Y. Zhao, *Nanophotonics* **2018**, *8*, 1; c) K. Robbie, G. Beydaghyan, T. Brown, C. Dean, J. Adams,

**ADVANCED
SCIENCE NEWS**

www.advancedsciencenews.com

**ADVANCED
MATERIALS**

www.advmat.de

C. Buzea, *Rev. Sci. Instrum.* **2004**, *75*, 1089; d) B. Wang, H. Qi, Y. Chai, M. Li, M. Guo, M. Pan, H. Wang, Y. Cui, J. Shao, *Superlattices Microstruct.* **2016**, *90*, 87.

[71] K. Robbie, M. J. Brett, *J. Vac. Sci. Technol., A* **1997**, *15*, 1460.

[72] K. Robbie, M. J. Brett, A. Lakhtakia, *Nature* **1996**, *384*, 616.

[73] A. C. van Popta, J. C. Sit, M. J. Brett, *Appl. Opt.* **2004**, *43*, 3632.

[74] L. Hu, P. Wang, X. Wan, S. Jiang, *J. Mater. Sci. Technol.* **2012**, *28*, 97.

[75] S. Wang, X. Zhao, Z. Fan, J. Shao, *Appl. Phys. A* **2012**, *107*, 227.

[76] R. Figueroa, T. G. S. Cruz, A. Gorenstein, *J. Power Sources* **2007**, *172*, 422.

[77] Q. Xie, W.-P. Wang, Z. Xie, P. Zhan, Z.-C. Li, Z.-J. Zhang, *Chin. Phys. B* **2015**, *24*, 057503.

[78] L.-C. Chen, C.-H. Tien, L. Xuguang, X. Bingshe, *J. Nanomater.* **2012**, *2012*, 105.

[79] Y. J. Park, K. M. A. Sobahan, C. K. Hwangbo, *Opt. Express* **2008**, *16*, 5186.

[80] C.-W. Chen, H.-W. Tsai, Y.-C. Wang, T.-Y. Su, C.-H. Yang, W.-S. Lin, Z.-H. Lin, J.-S. Huang, Y.-L. Chueh, *J. Mater. Chem. A* **2019**, *7*, 11452.

[81] B. D. Karahan, K. Amine, *J. Appl. Electrochem.* **2019**, *49*, 671.

[82] M. Chundak, I. Khalakhan, P. Kúš, T. Duchoň, V. Potin, A. Cacucci, N. Tsud, V. Matolín, K. Veltruská, *Mater. Chem. Phys.* **2019**, *232*, 485.

[83] M. A. Camblor, A. Corma, J. Pérez-Pariente, *Zeolites* **1993**, *13*, 82.

[84] J. M. Newsam, M. M. J. Treacy, W. T. Koetsier, C. B. D. Gruyter, *Proc. R. Soc. London, Ser A* **1988**, *420*, 375.

[85] J. B. Higgins, R. B. LaPierre, J. L. Schlenker, A. C. Rohrman, J. D. Wood, G. T. Kerr, W. J. Rohrbaugh, *Zeolites* **1988**, *8*, 446.

[86] M. M. J. Treacy, J. M. Newsam, *Nature* **1988**, *332*, 249.

[87] L. Xu, C. Qin, X. Wang, Y. Wei, E. Wang, *Inorg. Chem.* **2003**, *42*, 7342.

[88] Y. Duan, X. Liu, L. Han, S. Asahina, D. Xu, Y. Cao, Y. Yao, S. Che, *J. Am. Chem. Soc.* **2014**, *136*, 7193.

[89] F. Meng, S. A. Morin, A. Forticaux, S. Jin, *Acc. Chem. Res.* **2013**, *46*, 1616.

[90] S. A. Morin, M. J. Bierman, J. Tong, S. Jin, *Science* **2010**, *328*, 476.

[91] S. Hacialioglu, F. Meng, S. Jin, *Chem. Commun.* **2012**, *48*, 1174.

[92] S. A. Morin, A. Forticaux, M. J. Bierman, S. Jin, *Nano Lett.* **2011**, *11*, 4449.

[93] S. Jin, M. J. Bierman, S. A. Morin, *J. Phys. Chem. Lett.* **2010**, *1*, 1472.

[94] C. A. Orme, A. Noy, A. Wierzbicki, M. T. McBride, M. Grantham, H. H. Teng, P. M. Dove, J. J. DeYoreo, *Nature* **2001**, *411*, 775.

[95] E. A. Kulp, J. A. Switzer, *J. Am. Chem. Soc.* **2007**, *129*, 15120.

[96] T. Sugawara, Y. Suwa, K. Ohkawa, H. Yamamoto, *Macromol. Rapid Commun.* **2003**, *24*, 847.

[97] W. Jiang, M. S. Pacella, D. Athanasiadou, V. Nelea, H. Vali, R. M. Hazen, J. J. Gray, M. D. McKee, *Nat. Commun.* **2017**, *8*, 15066.

[98] W. Jiang, M. S. Pacella, H. Vali, J. J. Gray, M. D. McKee, *Sci. Adv.* **2018**, *4*, eaas9819.

[99] a) K. R. Kloetstra, H. W. Zandbergen, J. C. Jansen, H. van Bekkum, *Microporous Mater.* **1996**, *6*, 287; b) J. Y. Ying, C. P. Mehnert, M. S. Wong, *Angew. Chem., Int. Ed.* **1999**, *38*, 56.

[100] Y. Ono, K. Nakashima, M. Sano, Y. Kanekiyo, K. Inoue, S. Shinkai, M. Sano, J. Hojo, *Chem. Commun.* **1998**, 1477.

[101] a) J. H. Jung, G. John, M. Masuda, K. Yoshida, S. Shinkai, T. Shimizu, *Langmuir* **2001**, *17*, 7229; b) J. H. Jung, K. Yoshida, T. Shimizu, *Langmuir* **2002**, *18*, 8724.

[102] R. Oda, I. Huc, S. J. Candau, *Angew. Chem., Int. Ed.* **1998**, *37*, 2689.

[103] T. Delclos, C. Aimé, E. Pouget, A. Brizard, I. Huc, M.-H. Delville, R. Oda, *Nano Lett.* **2008**, *8*, 1929.

[104] a) Y. Sang, M. Liu, *Mol. Syst. Des. Eng.* **2019**, *4*, 11; b) J. H. Jung, Y. Ono, K. Hanabusa, S. Shinkai, *J. Am. Chem. Soc.* **2000**, *122*, 5008; c) Y. Ono, K. Nakashima, M. Sano, J. Hojo, S. Shinkai, *J. Mater. Chem.* **2001**, *11*, 2412.

[105] X. Wu, H. Jin, Z. Liu, T. Ohsuna, O. Terasaki, K. Sakamoto, S. Che, *Chem. Mater.* **2006**, *18*, 241.

[106] X. Wu, J. Ruan, T. Ohsuna, O. Terasaki, S. Che, *Chem. Mater.* **2007**, *19*, 1577.

[107] H. Qiu, S. Wang, W. Zhang, K. Sakamoto, O. Terasaki, Y. Inoue, S. Che, *J. Phys. Chem. C* **2008**, *112*, 1871.

[108] G.-L. Lin, Y.-H. Tsai, H.-P. Lin, C.-Y. Tang, C.-Y. Lin, *Langmuir* **2007**, *23*, 4115.

[109] J. Wang, W. Wang, P. Sun, Z. Yuan, B. Li, Q. Jin, D. Ding, T. Chen, *J. Mater. Chem.* **2006**, *16*, 4117.

[110] L. Zhou, G. Hong, L. Qi, Y. Lu, *Langmuir* **2009**, *25*, 6040.

[111] L. Zhao, P. Yuan, N. Liu, Y. Hu, Y. Zhang, G. Wei, L. Zhou, X. Zhou, Y. Wang, C. Yu, *J. Phys. Chem. B* **2009**, *113*, 16178.

[112] R. Atluri, N. Hedin, A. E. Garcia-Bennett, *J. Am. Chem. Soc.* **2009**, *131*, 3189.

[113] B. Liu, L. Han, S. Che, *Angew. Chem., Int. Ed.* **2012**, *51*, 923.

[114] H. Qiu, Y. Inoue, S. Che, *Angew. Chem., Int. Ed.* **2009**, *48*, 3069.

[115] K. Banerjee-Ghosh, O. Ben Dor, F. Tassinari, E. Capua, S. Yochelis, A. Capua, S.-H. Yang, S. S. P. Parkin, S. Sarkar, L. Kronik, L. T. Baczewski, R. Naaman, Y. Paltiel, *Science* **2018**, *360*, 1331.

[116] Y. Yang, M. Suzuki, S. Owa, H. Shirai, K. Hanabusa, *Chem. Commun.* **2005**, 4462.

[117] Z. Qinghong, L. Fei, L. Changli, W. Ye, W. Huilin, *Chem. Lett.* **2006**, *35*, 190.

[118] H. Jin, H. Qiu, Y. Sakamoto, P. Shu, O. Terasaki, S. Che, *Chem. - Eur. J.* **2008**, *14*, 6413.

[119] J. H. Jung, H. Kobayashi, K. J. C. van Bommel, S. Shinkai, T. Shimizu, *Chem. Mater.* **2002**, *14*, 1445.

[120] S. Liu, L. Han, Y. Duan, S. Asahina, O. Terasaki, Y. Cao, B. Liu, L. Ma, J. Zhang, S. Che, *Nat. Commun.* **2012**, *3*, 1215.

[121] C. Wang, S. Liu, Y. Duan, Z. Huang, S. Che, *Sci. Technol. Adv. Mater.* **2015**, *16*, 054206.

[122] K. E. Shopsowitz, A. Stahl, W. Y. Hamad, M. J. MacLachlan, *Angew. Chem., Int. Ed.* **2012**, *51*, 6886.

[123] K. M. Krause, M. J. Brett, *Adv. Funct. Mater.* **2008**, *18*, 3111.

[124] G. D. Gesesse, C. Li, E. Paineau, Y. Habibi, H. Remita, C. Colbeau-Justin, M. N. Ghazzal, *Chem. Mater.* **2019**, *31*, 4851.

[125] Z. R. Tian, J. A. Voigt, J. Liu, B. McKenzie, M. J. McDermott, *J. Am. Chem. Soc.* **2002**, *124*, 12954.

[126] X. Y. Kong, Y. Ding, R. Yang, Z. L. Wang, *Science* **2004**, *303*, 1348.

[127] a) X. Y. Kong, Z. L. Wang, *Appl. Phys. Lett.* **2004**, *84*, 975; b) M.-Q. Zhao, Q. Zhang, W. Fei, in *Advanced Hierarchical Nanostructured Materials* (Eds: Q. Zhang, F. Wei), Wiley-VCH, Weinheim, Germany **2014**, p. 193; c) Z. L. Wang, *Mater. Today* **2004**, *7*, 26.

[128] H. Gao, X. Zhang, M. Zhou, E. Zhang, Z. Zhang, *Solid State Commun.* **2006**, *140*, 455.

[129] W. Xiang, C. Wei, Q. Feng-Yu, *Chin. Phys. B* **2009**, *18*, 1669.

[130] a) X. Y. Kong, Z. L. Wang, *Nano Lett.* **2003**, *3*, 1625; b) P. X. Gao, W. Mai, Z. L. Wang, *Nano Lett.* **2006**, *6*, 2536.

[131] Z. C. Tu, X. Hu, *Phys. Rev. B* **2006**, *74*, 035434.

[132] J. Lin, B. Huang, Y. Dai, J. Wei, Y. Chen, *Mater. Sci. Eng., C* **2018**, *93*, 739.

[133] J. A. Switzer, H. M. Kothari, P. Poizot, S. Nakanishi, E. W. Bohannan, *Nature* **2003**, *425*, 490.

[134] R. Widmer, F.-J. Haug, P. Ruffieux, O. Gröning, M. Bielmann, P. Gröning, R. Fasel, *J. Am. Chem. Soc.* **2006**, *128*, 14103.

[135] M. Ortega Lorenzo, C. J. Baddeley, C. Muryn, R. Raval, *Nature* **2000**, *404*, 376.

[136] Y. Wang, H. Li, W. Qi, Y. Yang, Y. Yan, B. Li, L. Wu, *J. Mater. Chem.* **2012**, *22*, 9181.

[137] a) D.-Y. Du, L.-K. Yan, Z.-M. Su, S.-L. Li, Y.-Q. Lan, E.-B. Wang, *Coord. Chem. Rev.* **2013**, *257*, 702; b) B. Hasenknopf, K. Micoine, E. Lacôte, S. Thorimbert, M. Malacria, R. Thouvenot, *Eur. J. Inorg. Chem.* **2008**, *2008*, 5001; c) J. Crassous, *Chem. Soc. Rev.* **2009**, *38*, 830.

**ADVANCED
SCIENCE NEWS**

www.advancedsciencenews.com

**ADVANCED
MATERIALS**

www.advmat.de

[138] a) C. J. Besecker, V. W. Day, W. G. Klemperer, M. R. Thompson, *J. Am. Chem. Soc.* **1984**, *106*, 4125; b) V. W. Day, W. G. Klemperer, C. Schwartz, *J. Am. Chem. Soc.* **1987**, *109*, 6030; c) C. J. Besecker, V. W. Day, W. G. Klemperer, M. R. Thompson, *Inorg. Chem.* **1985**, *24*, 44.

[139] M. Inoue, T. Yamase, *Bull. Chem. Soc. Jpn.* **1995**, *68*, 3055.

[140] J. Iijima, H. Naruke, T. Sanji, *Inorg. Chem.* **2018**, *57*, 13351.

[141] C. Yvon, A. J. Surman, M. Hutin, J. Alex, B. O. Smith, D.-L. Long, L. Cronin, *Angew. Chem., Int. Ed.* **2014**, *53*, 3336.

[142] Z. Xiao, B. Huang, Y. Wang, Y. Chen, T. Zhai, X. Hu, D. Ke, P. Wu, *J. Cluster Sci.* **2019**, *30*, 837.

[143] H.-Y. An, E.-B. Wang, D.-R. Xiao, Y.-G. Li, Z.-M. Su, L. Xu, *Angew. Chem., Int. Ed.* **2006**, *45*, 904.

[144] X. Fang, T. M. Anderson, C. L. Hill, *Angew. Chem., Int. Ed.* **2005**, *44*, 3540.

[145] Y.-Q. Lan, S.-L. Li, Z.-M. Su, K.-Z. Shao, J.-F. Ma, X.-L. Wang, E.-B. Wang, *Chem. Commun.* **2008**, 58.

[146] J. Zhang, J. Hao, Y. Wei, F. Xiao, P. Yin, L. Wang, *J. Am. Chem. Soc.* **2010**, *132*, 14.

[147] S. T. Zheng, J. Zhang, G. Y. Yang, *Angew. Chem., Int. Ed.* **2008**, *47*, 3909.

[148] J. Crassous, *Chem. Commun.* **2012**, *48*, 9684.

[149] W. Xuan, R. Pow, N. Watfa, Q. Zheng, A. J. Surman, D.-L. Long, L. Cronin, *J. Am. Chem. Soc.* **2019**, *141*, 1242.

[150] C. Feng, K. C. Khulbe, T. Matsuura, R. Farnood, A. F. Ismail, *J. Membr. Sci. Res.* **2015**, *1*, 49.

[151] V. Soghomonian, Q. Chen, R. C. Haushalter, J. Zubieta, C. J. O'Connor, *Science* **1993**, *259*, 1596.

[152] J. Sun, C. Bonneau, Á. Cantín, A. Corma, M. J. Díaz-Cabañas, M. Moliner, D. Zhang, M. Li, X. Zou, *Nature* **2009**, *458*, 1154.

[153] T. Lu, W. Yan, R. Xu, *Inorg. Chem. Front.* **2019**, *6*, 1938.

[154] J. Yu, R. Xu, *J. Mater. Chem.* **2008**, *18*, 4021.

[155] a) M. E. Davis, R. F. Lobo, *Chem. Mater.* **1992**, *4*, 756; b) C. B. Dartt, M. E. Davis, *Catal. Today* **1994**, *19*, 151.

[156] M. Tong, D. Zhang, W. Fan, J. Xu, L. Zhu, W. Guo, W. Yan, J. Yu, S. Qiu, J. Wang, F. Deng, R. Xu, *Sci. Rep.* **2015**, *5*, 11521.

[157] G. Zhang, B. Wang, W. Zhang, M. Li, Z. Tian, *Dalton Trans.* **2016**, *45*, 6634.

[158] T. Lu, L. Zhu, X. Wang, W. Yan, W. Shi, R. Xu, *Inorg. Chem. Front.* **2018**, *5*, 1640.

[159] F. Daeyaert, M. W. Deem, *ChemistrySelect* **2019**, *4*, 3531.

[160] a) J. T. Collins, C. Kuppe, D. C. Hooper, C. Sibilia, M. Centini, V. K. Valev, *Adv. Opt. Mater.* **2017**, *5*, 1700182; b) X. Ma, M. Pu, X. Li, Y. Guo, P. Gao, X. Luo, *Nanomaterials* **2017**, *7*, 239.

[161] a) B. Banerjee, G. Misra, M. T. Ashraf, in *Data Processing Handbook for Complex Biological Data Sources* (Ed: G. Misra), Academic Press, MA, USA **2019**, p. 21; b) B. Ranjbar, P. Gill, *Chem. Biol. Drug Des.* **2009**, *74*, 101.

[162] Y. Duan, L. Han, J. Zhang, S. Asahina, Z. Huang, L. Shi, B. Wang, Y. Cao, Y. Yao, L. Ma, C. Wang, R. K. Dukor, L. Sun, C. Jiang, Z. Tang, L. A. Nafie, S. Che, *Angew. Chem., Int. Ed.* **2015**, *54*, 15170.

[163] a) S. Motojima, M. Kawaguchi, K. Nozaki, H. Iwanaga, *Carbon* **1991**, *29*, 379; b) S. Motojima, M. Kawaguchi, K. Nozaki, H. Iwanaga, *Appl. Phys. Lett.* **1990**, *56*, 321.

[164] D. L. Liu, D. X. Ye, F. Khan, F. Tang, B. K. Lim, R. C. Picu, G. C. Wang, T. M. Lu, *J. Nanosci. Nanotechnol.* **2003**, *3*, 492.

[165] J.-F. Lambert, *Origins Life Evol. Biospheres* **2008**, *38*, 211.

[166] K. B. Ghosh, W. Zhang, F. Tassinari, Y. Mastai, O. Lidor-Shalev, R. Naaman, P. Möllers, D. Nürenberg, H. Zacharias, J. Wei, E. Wierzbinski, D. H. Waldeck, *J. Phys. Chem. C* **2019**, *123*, 3024.

[167] D. Wang, Y. Li, G. Li Puma, C. Wang, P. Wang, W. Zhang, Q. Wang, *Chem. Commun.* **2013**, *49*, 10367.

[168] C. Zhang, Y. Li, D. Wang, W. Zhang, Q. Wang, Y. Wang, P. Wang, *Environ. Sci. Pollut. Res.* **2015**, *22*, 10444.

[169] Y. Zheng, L. Lin, X. Ye, F. Guo, X. Wang, *Angew. Chem., Int. Ed.* **2014**, *53*, 11926.

[170] S. Shaw, J. D. White, *Chem. Rev.* **2019**, *119*, 9381.

[171] A. J. Bendelsmith, S. C. Kim, M. Wasa, S. P. Roche, E. N. Jacobsen, *J. Am. Chem. Soc.* **2019**, *141*, 11414.

[172] C. Tan, J. Jiao, Z. Li, Y. Liu, X. Han, Y. Cui, *Angew. Chem., Int. Ed.* **2018**, *57*, 2085.

[173] T.-J. Yue, W.-M. Ren, L. Chen, G.-G. Gu, Y. Liu, X.-B. Lu, *Angew. Chem.* **2018**, *130*, 12852.

[174] a) G. Xu, C. H. Senanayake, W. Tang, *Acc. Chem. Res.* **2019**, *52*, 1101; b) A. J. Argüelles, S. Sun, B. G. Budaitis, P. Nagorny, *Angew. Chem., Int. Ed.* **2018**, *57*, 5325; c) K. Y. Wan, F. Roelfes, A. J. Lough, F. E. Hahn, R. H. Morris, *Organometallics* **2018**, *37*, 491; d) S. Luo, Z. Xiong, Y. Lu, Q. Zhu, *Org. Lett.* **2018**, *20*, 1837.

[175] I. Sato, K. Kadowaki, H. Urabe, J. H. Jung, Y. Ono, S. Shinkai, K. Soai, *Tetrahedron Lett.* **2003**, *44*, 721.

[176] Y. Ren, M. Wang, X. Chen, B. Yue, H. He, *Materials* **2015**, *8*, 1545.

[177] L. Zhang, S. Luo, J.-P. Cheng, *Catal. Sci. Technol.* **2011**, *1*, 507.

[178] H. Wang, T. Sakata, M. Azuma, T. Ohta, H. Takaya, *Chem. Lett.* **1990**, *19*, 1331.

[179] A. Hu, G. T. Yee, W. Lin, *J. Am. Chem. Soc.* **2005**, *127*, 12486.

[180] S. Kohtani, A. Kawashima, F. Masuda, M. Sumi, Y. Kitagawa, E. Yoshioka, Y. Hasegawa, H. Miyabe, *Chem. Commun.* **2018**, *54*, 12610.

[181] a) O. V. Fedorova, M. S. Valova, Y. A. Titova, I. G. Ovchinnikova, A. N. Grishakov, M. A. Uimin, A. A. Mysik, A. E. Ermakov, G. L. Rusinov, V. N. Charushin, *Kinet. Catal.* **2011**, *52*, 226; b) O. V. Fedorova, Y. A. Titova, A. Y. Vigorov, M. S. Toporova, O. A. Alisienok, A. N. Murashkevich, V. P. Krasnov, G. L. Rusinov, V. N. Charushin, *Catal. Lett.* **2016**, *146*, 493.

[182] a) G. K. E. Scriba, *Chromatographia* **2012**, *75*, 815; b) G. K. E. Scriba, in *Chiral Separations: Methods and Protocols* (Ed: G. K. E. Scriba), Springer, New York **2019**, p. 1.

[183] S. Xu, Y. Wang, Y. Tang, Y. Ji, *New J. Chem.* **2018**, *42*, 13520.

[184] A. Gogolashvili, E. Tatunashvili, L. Chankvetadze, T. Sohajda, J. Szeman, M. Gumustas, S. A. Ozkan, A. Salgado, B. Chankvetadze, *J. Chromatogr. A* **2018**, *1571*, 231.

[185] S. Adhikari, W. Lee, *J. Pharm. Invest.* **2018**, *48*, 225.

[186] B. Chankvetadze, in *Chiral Separations: Methods and Protocols* (Ed: G. K. E. Scriba), Springer, New York **2019**, p. 93.

[187] a) J. Wu, P. Su, J. Huang, S. Wang, Y. Yang, *J. Colloid Interface Sci.* **2013**, *399*, 107; b) Z.-S. Gong, L.-P. Duan, A.-N. Tang, *Microchim. Acta* **2015**, *182*, 1297; c) S. Xu, R. Mo, C. Jin, X. Cui, R. Bai, Y. Ji, *J. Pharm. Biomed. Anal.* **2017**, *140*, 190; d) X. Deng, W. Li, G. Ding, T. Xue, X. Chen, *Sep. Purif. Rev.* **2019**, *48*, 14; e) C. Chang, X. Wang, Y. Bai, H. Liu, *TrAC, Trends Anal. Chem.* **2012**, *39*, 195; f) A. K. Visheratina, F. Purcell-Milton, R. Serrano-García, V. A. Kuznetsova, A. O. Orlova, A. V. Fedorov, A. V. Baranov, Y. K. Gun'ko, *J. Mater. Chem. C* **2017**, *5*, 1692.

[188] Y. Fu, T. Huang, B. Chen, J. Shen, X. Duan, J. Zhang, W. Li, *Sep. Purif. Technol.* **2013**, *107*, 11.

[189] S. Ghosh, T. H. Fang, M. S. Uddin, K. Hidajat, *Colloids Surf., B* **2013**, *105*, 267.

[190] P. Yin, Z.-M. Zhang, H. Lv, T. Li, F. Haso, L. Hu, B. Zhang, J. Bacsa, Y. Wei, Y. Gao, Y. Hou, Y.-G. Li, C. L. Hill, E.-B. Wang, T. Liu, *Nat. Commun.* **2015**, *6*, 6475.

[191] a) X. Gao, B. Han, X. Yang, Z. Tang, *J. Am. Chem. Soc.* **2019**, *141*, 13700; b) X. Mao, H. Li, *J. Mater. Chem. B* **2013**, *1*, 4267.

[192] H. Sun, N. Gao, K. Dong, J. Ren, X. Qu, *ACS Nano* **2014**, *8*, 6202.

[193] Y. Ma, L. Shi, M. Zhou, B. Li, Z. Chen, L. Wu, *Chem. Commun.* **2019**, *55*, 7001.

[194] a) K. Saito, T. Tatsuma, *Nano Lett.* **2018**, *18*, 3209; b) J. Yeom, B. Yeom, H. Chan, K. W. Smith, S. Dominguez-Medina,

**ADVANCED
SCIENCE NEWS**

www.advancedsciencenews.com

**ADVANCED
MATERIALS**

www.advmat.de

Joong H. Bahng, G. Zhao, W.-S. Chang, S.-J. Chang, A. Chuvilin, D. Melnikau, A. L. Rogach, P. Zhang, S. Link, P. Král, N. A. Kotov, *Nat. Mater.* **2015**, *14*, 66.

[195] a) L. Lin, S. Lepeshov, A. Krasnok, T. Jiang, X. Peng, B. A. Korgel, A. Alù, Y. Zheng, *Mater. Today* **2019**, *25*, 10; b) F. Patti, R. Saija, P. Denti, G. Pellegrini, P. Biagioni, M. A. Iatì, O. M. Maragò, *Sci. Rep.* **2019**, *9*, 29; c) L. Lin, J. Zhang, X. Peng, Z. Wu, A. C. H. Coughlan, Z. Mao, M. A. Bevan, Y. Zheng, *Sci. Adv.* **2017**, *3*, e1700458.

[196] W. Feng, J.-Y. Kim, X. Wang, H. A. Calcaterra, Z. Qu, L. Meshi, N. A. Kotov, *Sci. Adv.* **2017**, *3*, e1601159.

[197] U. Hananel, A. Ben-Moshe, H. Diamant, G. Markovich, *Proc. Natl. Acad. Sci. USA* **2019**, *116*, 11159.

[198] W. J. Choi, G. Cheng, Z. Huang, S. Zhang, T. B. Norris, N. A. Kotov, *Nat. Mater.* **2019**, *18*, 820.

[199] X. Gao, X. Zhang, K. Deng, B. Han, L. Zhao, M. Wu, L. Shi, J. Lv, Z. Tang, *J. Am. Chem. Soc.* **2017**, *139*, 8734.

[200] a) S. Grimme, J. G. Brandenburg, C. Bannwarth, A. Hansen, *J. Chem. Phys.* **2015**, *143*, 054107; b) Y. Zhou, R. L. Marson, G. van Anders, J. Zhu, G. Ma, P. Ercius, K. Sun, B. Yeom, S. C. Glotzer, N. A. Kotov, *ACS Nano* **2016**, *10*, 3248.

[201] a) Y. Li, J. Cheng, J. Li, X. Zhu, T. He, R. Chen, Z. Tang, *Angew. Chem., Int. Ed.* **2018**, *57*, 10236; b) J.-i. Fujisawa, N. Kaneko, T. Eda, M. Hanaya, *Chem. Commun.* **2018**, *54*, 8490.

[202] Y. Tang, A. E. Cohen, *Phys. Rev. Lett.* **2010**, *104*, 163901.

[203] a) P. Patsalas, N. Kalfagiannis, S. Kassavetis, G. Abadias, D. V. Bellas, C. Lekka, E. Lidorikis, *Mater. Sci.Eng., R* **2018**, *123*, 1; b) G. V. Naik, J. Kim, A. Boltasseva, *Opt. Mater. Express* **2011**, *1*, 1090.

[204] H. Hu, Q. Gan, Q. Zhan, *Phys. Rev. Lett.* **2019**, *122*, 223901.

[205] a) A. O. Govorov, Z. Fan, P. Hernandez, J. M. Slocik, R. R. Naik, *Nano Lett.* **2010**, *10*, 1374; b) T. Hu, B. P. Isaacoff, J. H. Bahng, C. Hao, Y. Zhou, J. Zhu, X. Li, Z. Wang, S. Liu, C. Xu, J. S. Biteen, N. A. Kotov, *Nano Lett.* **2014**, *14*, 6799.

[206] G. Long, C. Jiang, R. Sabatini, Z. Yang, M. Wei, L. N. Quan, Q. Liang, A. Rasmita, M. Askerka, G. Walters, X. Gong, J. Xing, X. Wen, R. Quintero-Bermudez, H. Yuan, G. Xing, X. R. Wang, D. Song, O. Voznyy, M. Zhang, S. Hoogland, W. Gao, Q. Xiong, E. H. Sargent, *Nat. Photonics* **2018**, *12*, 528.

[207] Y. Zhao, A. Alù, *Nano Lett.* **2013**, *13*, 1086.

[208] J. P. Guillet, B. Recur, L. Frederique, B. Bousquet, L. Canioni, I. Manek-Hönninger, P. Desbarats, P. Mounaix, *J. Infrared, Millimeter, Terahertz Waves* **2014**, *35*, 382.

[209] C. Hao, G. Gao, Y. Li, L. Xu, M. Sun, C. Xu, H. Kuang, *Angew. Chem., Int. Ed.* **2019**, *58*, 7371.

[210] C. Hao, A. Qu, L. Xu, M. Sun, H. Zhang, C. Xu, H. Kuang, *J. Am. Chem. Soc.* **2019**, *141*, 1091.

[211] a) T. Vogl, R. Lecamwasam, B. C. Buchler, Y. Lu, P. K. Lam, *ACS Photonics* **2019**, *6*, 1955; b) W. Qin, L. Li, Z. Zhang, *Nat. Phys.* **2019**, *15*, 796; c) X. Liu, M. C. Hersam, *Nat. Rev. Mater.* **2019**, *4*, 669; d) J.-B. Qiao, Y. Gong, W.-J. Zuo, Y.-C. Wei, D.-L. Ma, H. Yang, N. Yang, K.-Y. Qiao, J.-A. Shi, L. Gu, L. He, *Phys. Rev. B* **2017**, *95*, 201403.

[212] a) R. Juchtmans, A. Béché, A. Abakumov, M. Batuk, J. Verbeeck, *Phys. Rev. B* **2015**, *91*, 094112; b) T. R. Harvey, F. S. Yasin, J. J. Chess, J. S. Pierce, R. M. S. dos Reis, V. B. Özdöl, P. Ercius, J. Ciston, W. Feng, N. A. Kotov, B. J. McMorran, C. Ophus, *Phys. Rev. Appl.* **2018**, *10*, 061001.

1906738 (28 of 28)